

Shape Optimization for the Mitigation of Coastal Erosion via Porous Shallow Water Equations

Luka Schlegel*, Volker Schulz*

CONTENTS

1	Introduction	3
2	Problem Formulation	4
2.1	PDE Constrained Optimization	4
3	Derivation of the Shape Derivative	7
3.1	Notations and Definitions	7
3.2	Shape Derivative	8
4	Numerical Results	11
4.1	SIPG-DG	11
4.2	Well-Balancedness of SIPG-DG for Porous SWE	12
4.3	Implementation Details for Shape Optimization	14
4.4	Example: The Half-Circled Mesh	16
5	Conclusion	17
A	Appendix	18
A.1	Derivation of Viscous Porous Momentum	18
A.2	Derivation of Adjoint Equations	19
A.3	Derivation of Shape Derivative	21
A.4	Derivation of DG Scheme for Interface Conditions	24
A.5	Numerical Convergence of the Smoothed Approach	25

LIST OF FIGURES

Figure 1	Illustrative Domain	4
Figure 2	Cross-Section of Wave and Sediment with Porous Region	5
Figure 3	Shape Optimization Algorithm	15
Figure 4	Ex. Mesh, Water Height, Velocities & Sediment	16
Figure 5	Ex. Optimized Shape & Close up	17
Figure 6	Ex. Target Functional	17
Figure 7	Examples of Smoothed Porosity	25

LIST OF TABLES

Table 1	Error Norms E_H and E_{uH} for decreasing α	26
---------	--	----

* *Department of Mathematics, University Trier, Trier, Germany*

ABSTRACT

Coastal erosion describes the displacement of land caused by destructive sea waves, currents or tides. Major efforts have been made to mitigate these effects using groins, breakwaters and various other structures. We address this problem by applying shape optimization techniques on the obstacles. We model the propagation of waves towards the coastline using two-dimensional viscous and porous Shallow Water Equations. The obstacle's shape, which is assumed to be permeable, is optimized over an appropriate cost function to minimize the height and velocities of water waves along the shore, without relying on a finite-dimensional design space, but based on shape calculus.

1 INTRODUCTION

Coastal erosion describes the displacement of land caused by destructive sea waves, currents or tides. Major efforts have been made to mitigate these effects using groins, breakwaters and various other structures. Among experimental set-ups to model the propagation of waves towards a shore and to find optimal wave-breaking obstacles, the focus has turned towards numerical simulations due to the continuously increasing computational performance. Calculating optimal shapes for various problems is a vital field, combining several areas of research. This paper builds up on the monographs [10][31][12] to perform free-form shape optimization. In addition, we strongly orientate on [29][30][28] that use the Lagrangian approach for shape optimization, i.e. calculating state, adjoint and the deformation of the mesh via the volume form of the shape derivative assembled on the right-hand-side of the linear elasticity equation, as Riesz representative of the shape derivative. Essential contributions to the field of numerical coastal protection have been made for steady [5][20][22] and unsteady [24][9][27] descriptions of propagating waves. In this paper we select one of the most widely applied system of wave equations. We describe the hydrodynamics by the set of Saint-Venant or better known as Shallow Water Equations (SWE), that originate from the famous Navier-Stokes Equations by depth-integrating, based on the assumption that horizontal length-scales are much larger than vertical ones [6]. To model a permeable obstacle, which can be exemplifying interpreted as a bag filled with sand, a porosity parameter is introduced. Porous SWE models are being paid increasing attention throughout the last decade, mostly because its ability to perform large-scale urban flood modelling [13]. Over the years a variety of models have been introduced differing in terms of conceptual, mathematical and numerical aspects. Our model mainly builds up on [17], such that we are dealing with a single, depth-independent porosity parameter in the definition of the SWE. In addition, we restrict ourself to isotropic porosity effects, such that the parameter cannot account for directional effects, which forms a legitimate assumption for a sand-filled obstacle. We would like to highlight that porous SWE have been modelled mainly by techniques relying on Finite Volume schemes. In this paper we calculate and derive numerical solutions to porous and viscous SWE via a Discontinuous Galerkin (DG) method for the advective and a Symmetric Interior Penalty Galerkin (SIPG) for the diffusive fluxes. To deal with numerical difficulties, that arise due to the discontinuous material coefficient, we extend the notion of a well-balanced DG scheme for classical SWE with discontinuous sediment [33] to porous, diffusive and two-dimensional SWE. In addition, we would like to highlight, that porous SWE have not been investigated in any kind of optimization yet, such that we firstly formulate adjoint and shape derivative for this set of equations and provide an algorithmic handle to this. The paper is structured as follows: In Section 2 we formulate the PDE-constrained optimization problem. In Section 3 we derive the necessary tools to solve this problem, by deriving adjoint equations and the shape derivative in volume form. The final part, Section 4, will present numerical techniques and applications of these results to a sample mesh.

2 PROBLEM FORMULATION

2.1 PDE Constrained Optimization

Suppose we are given an open domain $\tilde{\Omega} \subset \mathbb{R}^2$, which is split into the disjoint sets $\tilde{\Omega}, D \subset \Omega$ such that $\tilde{\Omega} \cup D \cup \Gamma_3 = \Omega$ and $\Gamma_1 \cup \Gamma_2 = \partial\Omega (=:\Gamma_{out})$. We assume the variable, interior boundary and the fixed outer $\partial\Omega$ to be at least Lipschitz. One simple example of such kind is visualized below in Figure 1.

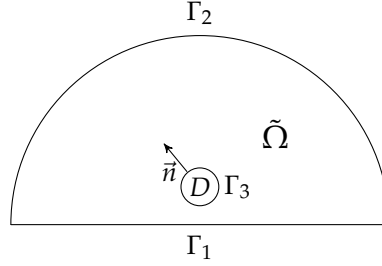


Figure 1: Illustrative Domain Ω with Initial Circled Obstacle D and Boundaries Γ_1, Γ_2 and Γ_3

On this domain we model water wave and velocity fields as the solution to viscous and porous SWE. We interpret $\Gamma_1, \Gamma_2, \Gamma_3$ as coastline, open sea and obstacle boundary and solve on $\Omega \times (0, T)$

$$\partial_t(\phi U) + \nabla \cdot (\phi F(U)) - \nabla \cdot (G(f(\phi, \epsilon)) \nabla \hat{U}) = \phi S(U) + S_\phi(U) \quad (1)$$

where we are given the SWE in vector notation with flux matrix F

$$F(U) = \left(\begin{array}{cc} \bar{Q} & \bar{Q} \\ \bar{Q} \otimes \bar{Q} + \frac{1}{2}gH^2\mathbf{I}_2 & \end{array} \right) = \left(\begin{array}{cc} Hu & vH \\ Hu^2 + \frac{1}{2}gH^2 & Huv \\ Huv & Hv^2 + \frac{1}{2}gH^2 \end{array} \right) \quad (2)$$

for identity matrix $\mathbf{I}_2 \in \mathbb{R}^{2 \times 2}$ and the solution of the form $U = (H, \bar{Q}) = (H, Hu, Hv)$, such as $\hat{U} = (H + z, \bar{Q})$, with H being the water height and Hu, Hv the weighted horizontal and vertical discharge or velocity and sediment height z . The porosity is a scalar function $\phi : \Omega \rightarrow (0, 1]$ representing the respective portion of space that is available to flow. We define

$$\phi \equiv \begin{cases} \phi_1 = \text{const. in } (\tilde{\Omega} \times (0, T)) \\ \phi_2 = \text{const. in } (D \times (0, T)) \end{cases} \quad (3)$$

The setting can be taken from Figure 2, where the region with differing porosity factor is exemplifying highlighted in grey.

We define the first source term in (1) as

$$S(U) = \begin{pmatrix} 0 \\ -gH \frac{\partial z}{\partial x} \\ -gH \frac{\partial z}{\partial y} \end{pmatrix} \quad (4)$$

responding to variations in the bed slope, where z is a scalar function for the height of the sediment. In addition, the parameter g represents the

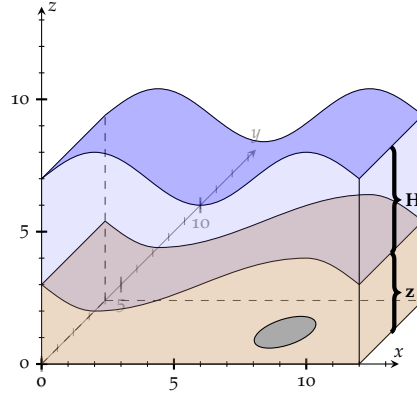


Figure 2: Cross-Section for Identification of Wave Height H , Sediment Height z and Porosity Coefficient ϕ

gravitational acceleration. The second source term in (1) corresponds to variations in the porosity coefficient and is chosen as [17]

$$S_\phi(U) = \begin{pmatrix} 0 \\ g \frac{H^2}{2} \frac{\partial \phi}{\partial x} \\ g \frac{H^2}{2} \frac{\partial \phi}{\partial y} \end{pmatrix} \quad (5)$$

For the SWE we employ outer boundary conditions as rigid-wall and non-reflecting boundary conditions for Γ_1 and Γ_2 as

$$\begin{aligned} \vec{Q} \cdot \vec{n} = 0, \nabla(H+z) \cdot \vec{n} = 0, \nabla Q_1 \cdot \vec{n} = 0, \nabla Q_2 \cdot \vec{n} = 0 & \quad \text{on } \Gamma_1 \times (0, T) \\ H = H_1, \nabla Q_1 \cdot \vec{n} = 0, \nabla Q_2 \cdot \vec{n} = 0 & \quad \text{on } \Gamma_2 \times (0, T) \end{aligned} \quad (6)$$

and transmissive interface conditions on $\Gamma_3 \times (0, T)$ for the continuity of the state

$$[[H+z]] = 0 \quad (7)$$

$$[[Q_1]] = 0 \quad (8)$$

$$[[Q_2]] = 0 \quad (9)$$

of the diffusive flux

$$[[\nabla(H+z) \cdot \vec{n}]] = 0 \quad (10)$$

$$[[\phi \nabla(Q_1) \cdot \vec{n}]] = 0 \quad (11)$$

$$[[\phi \nabla(Q_2) \cdot \vec{n}]] = 0 \quad (12)$$

and the advective flux

$$[[\phi F(U) \cdot \vec{n}]] = 0 \quad (13)$$

i.e.

$$[[\phi \vec{Q} \cdot \vec{n}]] = 0 \quad (14)$$

$$[[\{\phi Q_1/H + 1/2g\phi H^2; \phi Q_1 Q_2/H\} \cdot \vec{n}]] = 0 \quad (15)$$

$$[[\{\phi Q_1 Q_2/H; H v^2 + 1/2g\phi H^2\} \cdot \vec{n}]] = 0 \quad (16)$$

in addition we prescribe specific initial conditions on $\Omega \times \{0\}$ as

$$U = U_0 \quad (17)$$

Remark. To prevent shocks or discontinuities that can appear in the original formulation of the hyperbolic SWE even for continuous data in finite time, diffusive terms are added in (1) such that we obtain a set of fully parabolic equations. We control the amount of added diffusion by diagonal matrix $G(f(\phi, \epsilon)) = \sum_{i=1}^3 e_i^T f(\phi, \epsilon) e_i e_i^T$ with entries $f(\phi, \epsilon) = (\epsilon_v, \phi \epsilon_f, \phi \epsilon_f) \in \mathbb{R}_+^3$ and basis vector $e_i \in \mathbb{R}^n$ with n being the number of dimensions in vector $f(\phi, \epsilon)$. In this setting ϵ_f is fixed to a small value, while we rely on shock detection in the determination of ϵ_v following [26]. We refer to Section 4.4 for more detailed information.

Remark. A physical interpretation can be obtained for the introduction of the viscous part in the conservation of momentum equation [25]. However, diffusion in the continuity equation is solely based on stabilization arguments, we follow the justification as in [16].

Remark. So far only porous SWE, without additional viscous terms, have been introduced in the literature, hence the introduction is justified in appendix A.1. Instead of the derived non-linear formulation we will work with linear diffusion in the sense of artificial viscosity for simplicity. Commonly this is introduced to increase stability. We would like to highlight that adjoint-based shape optimization for non-linear diffusion can be handled in the same way, leading to additional terms in the adjoint equations and the shape derivative.

Remark. A constant porosity coefficient $\phi_1 = \phi_2$ in (1) leads to SWE in the classical form, that are subject for adjoint-based shape optimization in [27].

We finally obtain a PDE-constrained optimization problem by trying to meet certain predefined wave height and velocities \bar{U} at the shore Γ_1 weighted by diagonal matrix C such that we minimize objective $J_1 : \Omega \rightarrow \mathbb{R}$ where

$$J_1(\Omega) = \int_0^T \int_{\Gamma_1} \frac{1}{2} \|C(\hat{U}(t, x) - \bar{U}(t, x))\|^2 ds dt \quad (18)$$

This objective is supplemented by firstly a volume penalty, which hinders the obstacle from becoming arbitrarily large

$$J_2(\Omega) = \nu_1 \int_D 1 dx \quad (19)$$

secondly a perimeter regularization to ensure a sufficient regularity at obstacle level on Γ_3

$$J_3(\Omega) = \nu_2 \int_{\Gamma_3} 1 ds \quad (20)$$

and lastly a thickness control following [3]

$$J_4(\Omega) = \nu_3 \int_{\Gamma_3} \int_0^{d_{min}} [(d_\Omega(x - \zeta \vec{n}(x)))^+]^2 d\zeta ds \quad (21)$$

Here d_Ω represents the signed distance function with value

$$d_\Omega(x) = \begin{cases} d(x, \partial\tilde{\Omega}) & \text{if } x \in \tilde{\Omega} \\ 0 & \text{if } x \in \partial\tilde{\Omega} \\ -d(x, \partial\tilde{\Omega}) & \text{if } x \in \tilde{\Omega}^c \end{cases} \quad (22)$$

where the Euclidian distance of $x \in \mathbb{R}^d$ to a closed set $K \subset \mathbb{R}^d$ is defined as

$$d(x, K) = \min_{y \in K} \|x - y\| \quad (23)$$

for Euclidian distance $\|\cdot\|$. In order to hinder the obstacle from becoming arbitrarily large, we penalize its volume. To ensure a sufficient regularity at obstacle level, we are working with a perimeter regularization on Γ_3 . We would like to point out that the three penalty terms are controlled by parameters ν_1, ν_2 and ν_3 , which need to be defined a priori (for further details cf. to Section 3).

3 DERIVATION OF THE SHAPE DERIVATIVE

We now fix notations and definitions in the first part, before deriving the adjoint equations and shape derivatives in the second part, that are necessary to solve the PDE-constrained optimization problem.

3.1 Notations and Definitions

In this section we introduce a methodology that is commonly used in shape optimization, extensively elaborated in various works [10][31][12]. We fix notations and definitions following [30][28] and amend whenever it appears necessary. We start by introducing a family of mappings $\{\phi_\epsilon\}_{\epsilon \in [0, \tau]}$ for $\tau > 0$ that are used to map each current position $x \in \Omega$ to another by $\phi_\epsilon(x)$, where we choose the vector field \vec{V} as the direction for the so-called perturbation of identity

$$x_\epsilon = \phi_\epsilon(x) = x + \epsilon \vec{V}(x) \quad (24)$$

According to this methodology, we can map the whole domain Ω to another Ω_ϵ such that

$$\Omega_\epsilon = \phi_\epsilon(\Omega) = \{x_\epsilon | x + \epsilon \vec{V}(x), x \in \Omega\} \quad (25)$$

We define the Eulerian Derivative as

$$DJ(\Omega)[\vec{V}] = \lim_{\epsilon \rightarrow 0^+} \frac{J(\Omega_\epsilon) - J(\Omega)}{\epsilon} \quad (26)$$

Commonly, this expression is called shape derivative of J at Ω in direction \vec{V} and in this sense J shape differentiable at Ω if for all directions \vec{V} the Eulerian derivative exists and the mapping $\vec{V} \mapsto DJ(\Omega)[\vec{V}]$ is linear and continuous. In addition, we define the material derivative of some scalar function $p : \Omega_\epsilon \rightarrow \mathbb{R}$ at $x \in \Omega$ with respect to the deformation ϕ_ϵ as

$$D_m p(x) := \lim_{\epsilon \rightarrow 0^+} \frac{p \circ \phi_\epsilon(x) - p(x)}{\epsilon} = \frac{d^+}{d\epsilon} (p \circ \phi_\epsilon)(x) \Big|_{\epsilon=0} \quad (27)$$

and the corresponding shape derivative for a scalar p and a vector-valued \vec{P} for which the material derivative is applied component-wise as

$$Dp[\vec{V}] := D_m p - \vec{V} \cdot \nabla p \quad (28)$$

$$D\vec{P}[\vec{V}] := D_m \vec{P} - \vec{V}^T \nabla \vec{P} \quad (29)$$

In the following, we will use the abbreviation \dot{p} and \dot{P} to mark the material derivative of p and P . In Section 3 we will need to have the following calculation rules on board [7]

$$D_m(pq) = D_m p q + p D_m q \quad (30)$$

$$D_m \nabla p = \nabla D_m p - \nabla \vec{V}^T \nabla p \quad (31)$$

$$D_m \nabla \vec{P} = \nabla D_m \vec{P} - \nabla \vec{V}^T \nabla \vec{P} \quad (32)$$

$$D_m(\nabla q^T \nabla p) = \nabla D_m p^T \nabla q - \nabla q^T (\nabla \vec{V} + \nabla \vec{V}^T) \nabla p + \nabla p^T \nabla D_m q \quad (33)$$

In addition, the basic idea in the proof of the shape derivative in the next section will be to pull back each integral defined on the on the transformed field back to the original configuration. We therefore need to state the following rule for differentiating domain integrals [7]

$$\frac{d^+}{d\epsilon} \left(\int_{\Omega_\epsilon} p(\epsilon) \right) \Big|_{\epsilon=0} = \int_{\Omega} (D_m p + \nabla \cdot \vec{V} p) \quad (34)$$

3.2 Shape Derivative

We compute the adjoint equations and the shape derivative of the PDE-constrained optimization problem by formulating the Lagrangian

$$\mathcal{L}(\Omega, U, P) = J_1(\Omega) + a(U, P) - b(P) \quad (35)$$

where J_1 is the target functional (18), and $a(U, P)$ and $b(P)$ are obtained from boundary value problem (1). Here, we rewrite the equations in weak form by multiplying with some arbitrary test function $P \in H^1((0, T) \times \Omega)^3$ obtaining the form $a(U, P) = a(H, \vec{Q}, p, \vec{r})$ [1]

$$\begin{aligned} a(H, \vec{Q}, p, \vec{r}) := & \int_0^T \int_{\Omega} \left[\frac{\partial \phi H}{\partial t} + \nabla \cdot (\phi \vec{Q}) \right] p \, dx \, dt + \\ & \int_0^T \int_{\Omega} \epsilon_v \nabla (H + z) \cdot \nabla p \, dx \, dt - \int_0^T \int_{\Gamma_3} \llbracket \epsilon_v \nabla (H + z) \cdot \vec{n} p \rrbracket \, ds \, dt - \\ & \int_0^T \int_{\Gamma_2} \epsilon_v \nabla (H_1 + z) \cdot \vec{n} p \, ds \, dt + \\ & \int_0^T \int_{\Omega} \left[\frac{\partial \phi \vec{Q}}{\partial t} + \nabla \cdot \left(\phi \frac{\vec{Q}}{H} \otimes \vec{Q} + \frac{1}{2} g \phi H^2 \mathbf{I}_2 \right) \right] \cdot \vec{r} \, dx \, dt + \\ & \int_0^T \int_{\Omega} \epsilon_f \phi \nabla \vec{Q} : \nabla \vec{r} \, dx \, dt - \int_0^T \int_{\Gamma_3} \llbracket \phi \epsilon_f \nabla \vec{Q} \cdot \vec{n} \cdot \vec{r} \rrbracket \, ds \, dt + \\ & \int_0^T \int_{\Omega} g \phi H \nabla z \cdot \vec{r} \, dx \, dt - \int_0^T \int_{\Omega} g \frac{H^2}{2} \nabla \phi \cdot \vec{r} \, dx \, dt \end{aligned} \quad (36)$$

and a zero perturbation term.

Remark. To deal with well-defined weak forms and to allow us performing adjoint-based sensitivity analyses we assume the flow to be free of discontinuities, e.g. induced by a discontinuous bottom profile z or wave height H . In addition, we need to employ a specific handle to the discontinuous porosity coefficient. In this paper we have used the strategy to write each integral over Ω as the sum over subdomains $\int_{\Omega} = \int_{\tilde{\Omega}} + \int_D$. In (36) and in what follows this decomposition is assumed.

Remark. For the discontinuous coefficient we could rely on a smoothed porosity controlled by α , i.e. $\phi = \lim_{\alpha \rightarrow 0} \phi_\alpha$, e.g. by using smoothed cell transitions or mollifiers. In this setting we could integrate over the whole domain Ω . Such a handle would call for the necessity to show convergence results for state, adjoint and shape derivative. Furthermore we remark that a smoothing approach is presented in one dimension in appendix A.5 where we have used a smoothed step-function. Here interface conditions would not be required in the continuous form.

We obtain state equations from differentiating the Lagrangian w.r.t. P and the auxiliary problem, the adjoint equations, from differentiating the Lagrangian with respect to the states U . The adjoint is formulated in the following theorem:

Theorem 1. (Adjoint) Assume that the parabolic PDE problem (1) is H^1 -regular, so that its solution U is at least in $H^1((0, T) \times \Omega)^3$. Then the adjoint in strong form is given by

$$\phi \left[-\frac{\partial p}{\partial t} + \frac{1}{H^2} (\vec{Q} \cdot \nabla) \vec{r} \cdot \vec{Q} - gH(\nabla \cdot \vec{r}) + g\nabla z \cdot \vec{r} \right] - \nabla \cdot (\epsilon_v \nabla p) - gH \nabla \phi \cdot \vec{r} = -C_{11}((H+z) - \bar{H})_{\Gamma_1} \quad (37)$$

and

$$\phi \left[-\frac{\partial \vec{r}}{\partial t} - \nabla p - \frac{1}{H} (\vec{Q} \cdot \nabla) \vec{r} - \frac{1}{H} (\nabla \vec{r})^T \vec{Q} \right] - \nabla \cdot (\epsilon_f \phi \nabla \vec{r}) = -G(C_{22,33})(\vec{Q} - \vec{\bar{Q}})_{\Gamma_1} \quad (38)$$

with outer boundaries

$$\begin{aligned} p &= 0 & \text{in } \Omega \times \{T\} \\ \vec{r} &= 0 & \text{in } \Omega \times \{T\} \\ \vec{r} \cdot \vec{n} = 0, \nabla p \cdot \vec{n} = 0, \nabla r_1 \cdot \vec{n} = 0, \nabla r_2 \cdot \vec{n} = 0 & & \text{on } \Gamma_1 \times (0, T) \\ \phi p \vec{n} + \frac{\phi}{H_1} (\vec{Q} \cdot \vec{n}) \vec{r} + \frac{\phi}{H_1} (\vec{Q} \vec{r}) \cdot \vec{n} = 0, \nabla r_1 \cdot \vec{n} = 0, \nabla r_2 \cdot \vec{n} = 0 & & \text{on } \Gamma_2 \times (0, T) \end{aligned} \quad (39)$$

and interface boundaries on Γ_3 as

$$[[p]] = 0 \quad (40)$$

$$[[\vec{r}]] = 0 \quad (41)$$

such as

$$[[\nabla p \cdot \vec{n}]] = 0 \quad (42)$$

$$[[\phi \nabla r_1 \cdot \vec{n}]] = 0 \quad (43)$$

$$[[\phi \nabla r_2 \cdot \vec{n}]] = 0 \quad (44)$$

and

$$[[\phi F_U(P) \cdot \vec{n}]] = 0 \quad (45)$$

i.e.

$$[[\phi \left(\frac{\vec{Q}}{H^2} \cdot \vec{r} \vec{Q} + gH\vec{r} \right) \cdot \vec{n}]] = 0 \quad (46)$$

$$[[\phi (p + 2Q_1/Hr_1 + Q_2/Hr_2; Q_2/Hr_1) \cdot \vec{n}]] = 0 \quad (47)$$

$$[[\phi (Q_1/Hr_1; p + 2Q_2/Hr_2 + Q_1/Hr_2) \cdot \vec{n}]] = 0 \quad (48)$$

Proof. See Appendix A.2 □

The porous SWE adjoint can be written in vector form as

$$-\phi \frac{\partial P}{\partial t} + \phi A P_x + \phi B P_y + \phi C P - \nabla \cdot (G(f(\phi, \epsilon)) \nabla P) = S \quad (49)$$

where

$$A = \begin{pmatrix} 0 & \frac{\vec{Q}_1}{H^2} - gH & \frac{\vec{Q}_1 \vec{Q}_2}{H^2} \\ -1 & -2\frac{\vec{Q}_1}{H} & -\frac{\vec{Q}_2}{H} \\ 0 & 0 & -\frac{\vec{Q}_1}{H} \end{pmatrix}, \quad B = \begin{pmatrix} 0 & \frac{\vec{Q}_1 \vec{Q}_2}{H^2} & \frac{\vec{Q}_2^2}{H^2} - gH \\ 0 & -\frac{\vec{Q}_2}{H} & 0 \\ -1 & -\frac{\vec{Q}_1}{H} & -2\frac{\vec{Q}_2}{H} \end{pmatrix} \quad (50)$$

and C originates from variations in the sediment and the porosity such that

$$C = \begin{pmatrix} 0 & g \frac{\partial z}{\partial x} - g \frac{H}{\phi} \frac{\partial \phi}{\partial x} & g \frac{\partial z}{\partial y} - g \frac{H}{\phi} \frac{\partial \phi}{\partial y} \\ 0 & 0 & 0 \\ 0 & 0 & 0 \end{pmatrix} \quad (51)$$

Remark. In this paper, we will only consider the volume form of the shape derivative, which will be used to obtain smooth mesh deformations by a Riesz projection.

Theorem 2. (*Shape Derivative*) Assume that the parabolic PDE problem (1) is H^1 -regular, so that its solution U is at least in $H^1((0, T) \times \Omega)^3$. Moreover, assume that the adjoint equations (37) and (37) admit a solution $P \in H^1((0, T) \times \Omega)^3$. Then the shape derivative of the objective J (without volume and thickness penalty such as perimeter regularization) at Ω in the direction \vec{V} is given by

$$\begin{aligned} DJ_1(\Omega)[\vec{V}] = & \int_0^T \int_{\Omega} \left[-(\nabla \vec{V})^T : \nabla(\phi \vec{Q})p - (\nabla \vec{V})^T : \nabla \vec{Q} \frac{\phi \vec{Q}}{H} \cdot \vec{r} - \right. \\ & (\nabla \vec{V} \vec{Q} \cdot \nabla) \frac{\phi \vec{Q}}{H} \cdot \vec{r} - gH(\nabla \vec{V})^T \nabla(\phi H) \cdot \vec{r} - \\ & \epsilon_v \nabla(H+z)^T (\nabla \vec{V} + \nabla \vec{V}^T) \nabla p - \\ & \phi \epsilon_f \nabla \vec{Q} \nabla \vec{V} : \nabla \vec{r} - \phi \epsilon_f \nabla \vec{Q} \nabla \vec{V}^T : \nabla \vec{r} - \\ & g\phi H \nabla \vec{V}^T \nabla z \cdot \vec{r} + \frac{1}{2} g H^2 \nabla \vec{V}^T \nabla \phi \cdot \vec{r} \\ & \left. \operatorname{div}(\vec{V}) \left\{ \frac{\partial \phi H}{\partial t} p + \nabla \cdot (\phi \vec{Q})p + \frac{\partial \phi \vec{Q}}{\partial t} \cdot \vec{r} + \right. \right. \\ & \phi(\vec{Q} \cdot \nabla) \frac{\vec{Q}}{H} \cdot \vec{r} + \nabla \cdot (\phi \vec{Q}) \frac{\vec{Q}}{H} \cdot \vec{r} + \frac{1}{2} g \nabla(\phi H^2) \cdot \vec{r} + \\ & g\phi H \nabla z \cdot \vec{r} + \epsilon_v \nabla(H+z) \cdot \nabla p + \\ & \left. \left. \phi \epsilon_f \nabla \vec{Q} : \nabla \vec{r} - g \frac{1}{2} H^2 \nabla \phi \cdot \vec{r} \right\} \right] dx dt \end{aligned} \quad (52)$$

Proof. See Appendix A.3 □

The shape derivatives of the penalty terms (volume, perimeter and thickness) are obtained as, see e.g. [31][32]

$$DJ_2 = \nu_1 \int_{\Omega} \operatorname{div}(\vec{V}) dx \quad (53)$$

$$DJ_3 = \nu_2 \int_{\Gamma_3} \kappa \langle \vec{V}, \vec{n} \rangle ds = \nu_2 \int_{\Gamma_3} \nabla \cdot \vec{V} - \langle \frac{\partial \vec{V}}{\partial \vec{n}}, \vec{n} \rangle ds \quad (54)$$

and see [3] for

$$\begin{aligned} DJ_4 = \nu_3 \int_{\Gamma_3} \int_0^{d_{\min}} & \left[\vec{V}(x) \vec{n}(x) \left\{ \kappa(x) (d_{\Omega}(x_m)^+)^2 + 2d_{\Omega}(x_m)^+ \nabla d_{\Omega}(x_m) \cdot \nabla d_{\Omega}(x) \right\} - \right. \\ & \left. \vec{V}(p_{\partial\Omega}(x_m)) \cdot \vec{n}(p_{\partial\Omega}(x_m)) 2(d_{\Omega}(x_m))^+ \right] d\zeta ds \end{aligned} \quad (55)$$

for curvature κ and offset point $x_m = x - \zeta \vec{n}(x)$, where we require the shape derivative of the signed distance function [12]

$$d'_{\Omega}(V)(x) = -\vec{V}(p_{\partial\Omega}(x)) \cdot \vec{n}(p_{\partial\Omega}(x)) \quad (56)$$

with operator $p_{\partial\Omega}$ that projects a point $x \in \Omega$ onto its closest boundary and holds for all $x \notin \Sigma$, where Σ is referred to as the ridge, where the minimum in (23) is obtained by two distinct points.

4 NUMERICAL RESULTS

In the first part of this section we shortly sketch the SIPG-DG method as in [18], before we discuss the well-balancedness of the porous, viscous SWE and describing the algorithm for shape optimization in detail.

4.1 SIPG-DG

We solve the boundary value problem (1) and the adjoint problem (37) and (38) with the finite element solver FEniCS. For the time discretization we can choose between Euler and Runge-Kutta schemes. High accuracy even for the inviscid and hyperbolic PDE, i.e. $\epsilon = 0$, is achieved using a Discontinuous Galerkin (DG) method to discretize in space [2][21][23]. This implies discontinuous cell transitions, and hence a formulation based on each element $\kappa \in \mathcal{T}_h$ or facet Γ_I for a subdivision \mathcal{T}_h of some mesh Ω , such as a redefinition of each function and operator on the so-called broken and possibly vector-valued d -dimensional Sobolov space $\mathcal{H}^m((0, T) \times \mathcal{T}_h)^d$. In this light, we also need to define the average $\{\{U\}\} = (U^+ + U^-)/2$ and jump term $\llbracket U \rrbracket = U^+ \otimes n_+ + U^- \otimes n_-$ to express fluxes on cell transitions. The discretization then reads for solution and test-function $U_h, P_h \in \mathcal{H}^1((0, T) \times \mathcal{T}_h)^3$ as [18][19]

$$\begin{aligned}
 N_h(U_h, P_h) = & \int_0^T \int_{\Omega} \left[\frac{\partial \phi_h U_h}{\partial t} \cdot P_h - \phi_h F(U_h) : \nabla_h P_h + G(f(\phi_h, \epsilon)) \nabla_h(\hat{U}_h) : \nabla_h P_h - \right. \\
 & \left. \phi_h S(U_h) \cdot P_h - S_{\phi_h}(U_h) \cdot P_h \right] dx dt + \\
 & \int_0^T \sum_{\kappa \in \mathcal{T}_h} \int_{\partial \kappa \setminus \Gamma} \mathcal{H}(U_h^{+,*}, U_h^{-,*}, \vec{n}^+) \cdot P_h^+ ds dt + \\
 & \int_0^T \int_{\Gamma_I} \left[\delta_h : \llbracket P_h \rrbracket ds dt - \{\{G(f(\phi_h, \epsilon)) \nabla_h(P_h)\}\} : \llbracket \hat{U}_h \rrbracket - \right. \\
 & \left. \{\{G(f(\phi_h, \epsilon)) \nabla_h(\hat{U}_h)\}\} : \llbracket P_h \rrbracket \right] ds dt + N_{\Gamma, h}(U_h, P_h, \phi_h)
 \end{aligned} \tag{57}$$

where the function \mathcal{H} defines the fluxes at the discontinuous cell transitions, incorporating specific values at the boundaries U_h^+, U_h^- . For the advective flux and for a given flux Jacobian $J_i := \partial_U F_i(U)$ and matrix $B(U, \vec{n}) = \sum_{i=1}^2 n_i J_i(U)$.

Remark. We can choose between a variety of fluxes [2], from here on the (Local) Lax-Friedrichs Flux is used that is defined as

$$\mathcal{H}(U^+, U^-, \vec{n})|_{\partial \kappa} = \frac{1}{2} (F(U^+) \cdot \vec{n} + F(U^-) \cdot \vec{n} + \alpha_{\max}(U^+ - U^-)) \tag{58}$$

where $\alpha_{\max} = \max_{V=U^+, U^-} \{|\lambda(B(V, \vec{n}_\kappa))|\}$ with $\lambda(B(V, \vec{n}_\kappa))$ returning a sequence of eigenvalues for the matrix B restricted on a side of element κ .

Remark. For the classical SWE eigenvalues of the SWE-Jacobian are obtained following [2], where $c = \sqrt{gH}$ denotes the wave celerity, as

$$\begin{aligned}
 \lambda(n_1 J_1 + n_2 J_2) &= \{\lambda_1, \lambda_2, \lambda_3\} \\
 &= \{un_1 + vn_2 - c, un_1 + vn_2, un_1 + vn_2 + c\}
 \end{aligned} \tag{59}$$

Remark. We would like to highlight, that the chosen interface condition, lead to a DG scheme for cells at the interface as well. Hence, the summation of all integrals of interior cell boundaries $\sum_{\kappa \in \mathcal{T}_h} \int_{\partial \kappa \setminus \Gamma}$ in (57) includes the interface boundary Γ_3 . We show this in appendix A.4.

In (57) we define the penalization term for the viscous fluxes as [18]

$$\delta_h(\hat{U}_h) = C_{IP} \frac{p^2}{h} \{ \{ G(f(\phi_h^+, \epsilon)) \} \} \llbracket \hat{U}_h \rrbracket \quad (60)$$

where $C_{IP} > 0$ is a constant, $p > 0$ the polynomial order of the DG method and $h > 0$ the ratio of the cell volume and the facet area. What is remaining in (57) is the specification of the boundary term, here we state that

$$\begin{aligned} N_{\Gamma,h}(U_h, P_h) = & \int_0^T \int_{\Gamma} \mathcal{H}(U_h^+, U_{\Gamma}(U_h^+), \vec{n}) \cdot P_h^+ \, ds \, dt + \\ & \int_0^T \int_{\Gamma_n} \left[\delta_{\Gamma}(U_h^+) : P_h^+ \otimes \vec{n}^+ + G(f(\phi_h^+, \epsilon)) \nabla_h(\hat{U}_h^+) : P_h^+ \otimes \vec{n} - \right. \\ & \left. G(f(\phi_h^+, \epsilon)) \nabla_h V_h^+ : (\hat{U}_h^+ - U_{\Gamma}(\hat{U}_h^+)) \otimes \vec{n} \right] \, ds \, dt \end{aligned} \quad (61)$$

where Γ_n are all boundaries of type Neumann. Additionally, we define

$$\delta_{\Gamma}(U_h^+) = C_{IP} G(f(\phi_h^+, \epsilon)) \frac{p^2}{h} (U_h^+ - U_{\Gamma}(U_h^+)) \otimes \vec{n} \quad (62)$$

$$\mathcal{H}(U_h^+, U_{\Gamma}(U_h^+), \vec{n}^+) = \frac{1}{2} [\vec{n}^+ \cdot F(U_h^+) + \vec{n}^+ \cdot F(U_{\Gamma}(U_h^+))] \quad (63)$$

For the pure advective SWE open and rigid-wall boundary functions are defined as [2].

4.2 Well-Balancedness of SIPG-DG for Porous SWE

Approximate numerical solutions to systems like (1), which allow to properly handle shocks and contact discontinuities, are in general known to be inaccurate even for near steady states [15]. This difficulty can be overcome by using the so-called well-balanced schemes, firstly introduced in [8]. We will derive this property for our numerical scheme for the case of one-dimensional equations extending the approach in [33] to porous SWE with diffusive terms. The two-dimensional formulation follows immediately then. Before starting we explicitly state that we rely our solver on variables

$$\tilde{U} = \begin{pmatrix} h \\ uh \end{pmatrix} = \begin{pmatrix} \phi H \\ \phi u H \end{pmatrix} \quad (64)$$

Hence we redefine the 1D porous SWE without diffusion in vector notation as

$$\partial_t(\tilde{U}) + \nabla \cdot (F(\tilde{U})) = S(\tilde{U}) + S_{\phi}(\tilde{U}) \quad (65)$$

for given flux matrix

$$F(\tilde{U}) = \begin{pmatrix} hu \\ hu^2 + \frac{1}{2}gh^2/\phi \end{pmatrix} \quad (66)$$

and as before a source regarding the variations in the sediment

$$S(\tilde{U}) = \begin{pmatrix} 0 \\ -gh \frac{\partial z}{\partial x} \end{pmatrix} \quad (67)$$

and variations in the porosity factor

$$S_{\phi}(\tilde{U}) = \begin{pmatrix} 0 \\ \frac{g}{2} \frac{h^2}{\phi^2} \frac{\partial \phi}{\partial x} \end{pmatrix} \quad (68)$$

Well-Balancing relies on incorporating the discretization of the source term in fluxes, that e.g. (58) used in (57) is redefined. Preserving still water stationary conditions means that $uh = 0$ for $h/\phi + z = C$ for all $t \in \{0, T\}$. For the contribution to time changes it should be justified that on each element $\kappa \in \mathcal{T}_h = [x_{j-1/2}, x_{j+1/2}]$

$$\begin{aligned} R = & - \int_{\kappa} F(\tilde{U}_h(x, t)) \cdot \partial_x P_h(x) \, dx + \mathcal{H}_{j+1/2}^L \cdot P_h(x_{j+1/2}^-) - \mathcal{H}_{j-1/2}^R \cdot P_h(x_{j-1/2}^+) \\ & - \int_{\kappa} S(\tilde{U}_h(x, t)) \cdot P_h(x) \, dx - \int_{\kappa} S_{\phi}(\tilde{U}_h(x, t)) \cdot P_h(x) \, dx = 0 \end{aligned} \quad (69)$$

In [33] it is stated that Equation (69) is fulfilled if,

1. $\mathcal{H}_{j+1/2}^L = F(\tilde{U}_h(x_{j+1/2}^-))$ and $\mathcal{H}_{j-1/2}^R = F(\tilde{U}_h(x_{j-1/2}^+))$
2. We are in a steady state and u_h is a numerical approximation of u , hence

$$\partial_x F(\tilde{U}_h) = \begin{pmatrix} 0 \\ g(h_h, z_h) \end{pmatrix} \quad (70)$$

The assumption above can be easily justified and shows the appropriateness of the unmodified scheme in case of continuous piecewise sediment $z_h(x_{j+1/2}^-) = z_h(x_{j+1/2}^+)$ and porosity coefficients $\phi_h(x_{j+1/2}^-) = \phi_h(x_{j+1/2}^+)$. Situations with discontinuous sediment are dealt by relying on the idea of redefining variables [4], i.e.

$$h_{h,j+1/2}^{+,*} = \max \left(0, h_{h,j+1/2}^+ + z_{h,j+1/2}^+ - \max(z_{h,j+1/2}^+, z_{h,j+1/2}^-) \right) \quad (71)$$

$$h_{h,j+1/2}^{-,*} = \max \left(0, h_{h,j+1/2}^- + z_{h,j+1/2}^- - \max(z_{h,j+1/2}^+, z_{h,j+1/2}^-) \right) \quad (72)$$

which can be extended for varying porosity coefficient to

$$\begin{aligned} h_{h,j+1/2}^{+,*} = & \max \left(0, \frac{h_{h,j+1/2}^+}{\phi_{h,j+1/2}^+} + z_{h,j+1/2}^+ - \max(z_{h,j+1/2}^+, z_{h,j+1/2}^-) \right) \min \left(\phi_{h,j+1/2}^+, \phi_{h,j+1/2}^- \right) \end{aligned} \quad (73)$$

$$\begin{aligned} h_{h,j+1/2}^{-,*} = & \max \left(0, \frac{h_{h,j+1/2}^-}{\phi_{h,j+1/2}^-} + z_{h,j+1/2}^- - \max(z_{h,j+1/2}^+, z_{h,j+1/2}^-) \right) \min \left(\phi_{h,j+1/2}^+, \phi_{h,j+1/2}^- \right) \end{aligned} \quad (74)$$

such that

$$\tilde{U}_{h,j+1/2}^{+,*} = \begin{pmatrix} h_{h,j+1/2}^{+,*} \\ uh_{h,j+1/2}^+ \end{pmatrix} \quad (75)$$

Theorem 3. Redefining $\tilde{U}_{h,j+1/2}^{\pm,*}$ as in (75) in accordance with corrector terms lead to a well-balanced scheme

Proof.

$$\begin{aligned} \mathcal{H}_{j+1/2}^L = & \mathcal{H}(\tilde{U}_{h,j+1/2}^{-,*}, \tilde{U}_{h,j+1/2}^{+,*}) \\ & + \begin{pmatrix} 0 \\ \frac{g}{2}(h_{h,j+1/2}^-)^2 / \phi_{h,j+1/2}^- - \frac{g}{2}(h_{h,j+1/2}^{-,*})^2 / \min(\phi_{h,j+1/2}^+, \phi_{h,j+1/2}^-) \end{pmatrix} \\ = & F(\tilde{U}_{h,j+1/2}^-) \end{aligned}$$

Similarly

$$\mathcal{H}_{j-1/2}^R = F(\tilde{U}_{h,j-1/2}^+)$$

□

Extending results to two dimensions can be done by looking at the residual on an element $\kappa \in \mathcal{T}_h$

$$\begin{aligned} R = & - \int_{\kappa} F(\tilde{U}_h(x, t)) : \nabla P_h(x) \, dx + \int_{\partial\kappa} \mathcal{H}_{\partial\kappa}(U_h^+(x, t), U_h^-(x, t), \vec{n}^+) \cdot P_h^+ \, ds \\ & - \int_{\kappa} S(\tilde{U}_h(x, t)) \cdot P_h(x) \, dx - \int_{\kappa} S_{\phi}(\tilde{U}_h(x, t)) \cdot P_h(x) \, dx = 0 \end{aligned} \quad (76)$$

and relying on a flux modification on each elemental boundary as

$$\mathcal{H}_{\partial\kappa} = \mathcal{H}(\tilde{U}_{h,\partial\kappa}^{-,*}, \tilde{U}_{h,\partial\kappa}^{+,*}, \vec{n}_{\partial\kappa}^+) \quad (77)$$

$$+ G \begin{pmatrix} 0 \\ \vec{n}_{0,\partial\kappa}^+ \\ \vec{n}_{1,\partial\kappa}^+ \end{pmatrix} \begin{pmatrix} 0 \\ \frac{g}{2}(h_{h,\partial\kappa}^+)^2 / \phi_{h,\partial\kappa}^+ - \frac{g}{2}(h_{h,\partial\kappa}^{+,*})^2 / \min(\phi_{h,\partial\kappa}^+, \phi_{h,\partial\kappa}^-) \\ \frac{g}{2}(h_{h,\partial\kappa}^+)^2 / \phi_{h,\partial\kappa}^+ - \frac{g}{2}(h_{h,\partial\kappa}^{+,*})^2 / \min(\phi_{h,\partial\kappa}^+, \phi_{h,\partial\kappa}^-) \end{pmatrix} \quad (78)$$

where

$$\tilde{U}_{h,\partial\kappa}^{+,*} = \begin{pmatrix} h_{h,\partial\kappa}^{+,*} \\ uh_{h,\partial\kappa}^+ \\ vh_{h,\partial\kappa}^+ \end{pmatrix} \quad (79)$$

Remark. Adding diffusive terms in the form

$$\partial_t(\tilde{U}) + \nabla \cdot (F(\tilde{U})) - \nabla \cdot (G(f(\phi, \epsilon))\nabla \hat{U}) = S(\tilde{U}) + S_{\phi}(\tilde{U})$$

where $\hat{U} = (z + h/\phi, uH, vH)$, does not disturb well-balancedness, since rest conditions cancel contributing terms.

Remark. Reformulation (64) requires eigenvalues in the form of (59) with $c = \sqrt{gh/\phi}$ to be used in the numerical flux function.

Remark. The numerical scheme used to handle discontinuous sediment and porosity coefficients forms the limit of a smoothed scenario, such that $U_{\alpha} \rightarrow U$ in $H^1((0, T) \times \Omega)^3$ where $\phi_{\alpha} \rightarrow \phi$ for $\alpha \rightarrow 0$ which is verified for one dimension numerically in appendix A.5.

4.3 Implementation Details for Shape Optimization

We rely on the classical structure of adjoint-based shape optimization algorithms shortly sketched in Figure 3.

The solution to the signed distance function is based on the solution of the Eikonal Equation with $f(x) = 1$, $q(x) = 0$

$$\begin{aligned} |\nabla w(x)| &= f(x) & x \in \Omega \\ w(x) &= q(x) & x \in \partial\Omega \end{aligned} \quad (80)$$

where we have implemented a viscous and stabilized version to obtain $w \in H^1(\Omega)$ for all $v \in H^1(\Omega)$ i.e.

$$\int_{\Omega} \sqrt{\nabla w \nabla w} v \, dx - \int_{\Omega} f v \, dx + \int_{\Omega} \epsilon_{SDF} \nabla w \nabla v \, dx = 0 \quad (81)$$

Algorithm 1: Shape Optimization Algorithm

```

Initialization
while  $\|DJ(\Omega_k)\| > \epsilon$  do
  1 Calculate SDF  $w_k$ 
  2 Calculate State  $U_k$  via  $\tilde{U}_k$ 
  3 Calculate Adjoint  $P_k$  via  $\tilde{P}_k$ 
  4 Use  $DJ_{1,2,3,4}(\Omega_k)[\vec{V}]$  to calculate Gradient  $W_k$ 
  5 Perform Linesearch for  $\tilde{W}_k$ 
  6 Deform  $\Omega_{k+1} \leftarrow \mathcal{D}_{\tilde{W}_k}(\Omega_k)$ 
end

```

Figure 3: Shape Optimization Algorithm

where $\epsilon_{SDF} = \max h_\kappa$ is dependent on the element-diameter h_κ of $\kappa \in \mathcal{T}_h$. Numerical solutions to the adjoint equations require us to rewrite the vector form (49) with the help of the product rule, i.e.

$$\frac{\partial P}{\partial t} - \nabla \cdot (AP, BP) - \tilde{C}P + \nabla \cdot (G(f(\phi, \epsilon))\nabla P) = -S \quad (82)$$

where \tilde{C} is defined to be

$$\tilde{C} = C - A_x - B_y \quad (83)$$

As we have shown in [27] the eigenvalues of matrix $B^*(P, \vec{n})$ belonging to the adjoint flux Jacobian $\mathcal{J}_i^* := \partial_P F_i^*(P)$ equal the eigenvalues of matrix $B(U, \vec{n})$ belonging to the flux Jacobian $\mathcal{J}_i := \partial_U F_i(U)$. The SWE adjoint problem is then solved in the same manner as the scheme for the forward system (4.1) with (4.2), using a well-balanced SIPG-DG discretization in space and a one-step Euler or Runge-Kutta scheme for the time discretization.

Updating the finite element mesh in each iteration is done via the solution $W : \Omega \rightarrow \mathbb{R}^2$ of the linear elasticity equation [30]

$$\begin{aligned} \int \sigma(W) : \epsilon(V) &= DJ[\vec{V}] & \forall \vec{V} \in H_0^1(\Omega, \mathbb{R}^2) \\ \sigma &:= \lambda_{elas} \text{Tr}(\epsilon(W))I + 2\mu_{elas}\epsilon(W) \\ \epsilon(W) &:= \frac{1}{2}(\nabla W + \nabla W^T) \\ \epsilon(V) &:= \frac{1}{2}(\nabla V + \nabla V^T) \end{aligned} \quad (84)$$

where σ and ϵ are called strain and stress tensor and λ_{elas} and μ_{elas} are called Lamé parameters. In our calculations we have chosen $\lambda_{elas} = 0$ and μ_{elas} as the solution of the following Poisson Problem

$$\begin{aligned} -\Delta \mu &= 0 & \text{in } \Omega \\ \mu &= \mu_{max} & \text{on } \Gamma_3 \\ \mu &= \mu_{min} & \text{on } \Gamma_1, \Gamma_2 \end{aligned} \quad (85)$$

The source term $DJ[\vec{V}]$ in (84) consists of a volume and surface part, i.e. $DJ[\vec{V}] = DJ_\Omega[\vec{V}] + DJ_{\Gamma_3}[\vec{V}]$.

Remark. The volumetric share comes from our SWE shape derivative and the penalty on the volume, where we only assemble for test vector fields whose support intersects with the interface Γ_3 and which are set to zero for all other basis vector fields. The surface part comes from the parameter regularization and the thickness constraint in (18).

Remark. To guarantee the attainment of useful shapes, which minimize the objective, a backtracking line search is used, which limits the step size in case the shape space is left [32] i.e. having intersecting line segments or in the case of a non-decreasing objective evaluation. As described in Figure 3 the iteration is finally stopped if the norm of the shape derivative has become sufficiently small.

4.4 Example: The Half-Circled Mesh

In the first example, we will look at the model problem - the half circle that was described in Section 2. As before, we interpret $\Gamma_1, \Gamma_2, \Gamma_3$ as coastline, open sea and obstacle boundary. We will work with a rest height of the water at $\bar{H} = 1$, while targeting zeroed velocities. We penalize volume and thinness by setting $\nu_1 = 0.0001, \nu_3 = 0.01$ and enforce a stronger regularization by $\nu_2 = 0.0001$. The parameters in the porous shallow water system are set as follows: For the weight of the diffusion terms in the momentum equation we set $\epsilon_f = 0.01$ and determine ϵ_v by the usage of the mentioned shock detector [26]. The gravitational acceleration is fixed at roughly 9.81. The mesh is displayed in Figure 4 and was created using the finite element mesh generator GMSH [14], we have meshed finer around the obstacle to ensure a high resolution. The material coefficient is at $\phi_2 = 0.5$ at D and we obtain classical SWE on $\tilde{\Omega}$ by setting $\phi_1 = 1$. In addition, we employ Gaussian initial conditions as $(H_0 + z, uH_0, vH_0) = (1 + \exp(-15x^2 - 15(y-1)^2), 0, 0)$, which result into a wave travelling in time towards the boundaries. We prescribe the boundary conditions as before, using rigid-wall and outflow boundary conditions for Γ_1 and Γ_2 . In this example we have used a forward

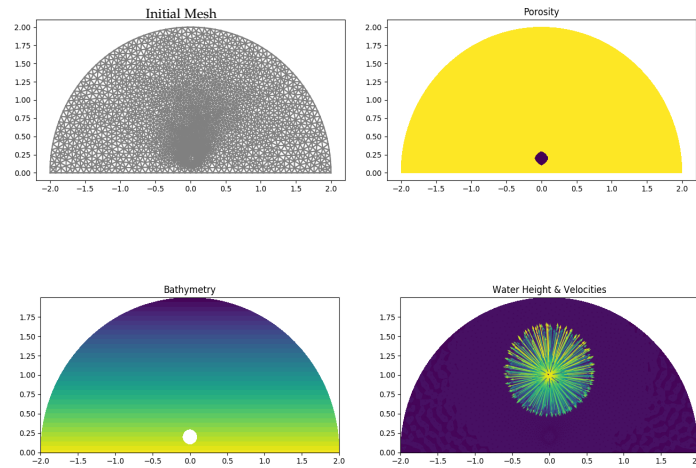


Figure 4: 1.: Initial Mesh Ω_h , 2.: Initial Shape of Porosity Coefficient ϕ , 3.: Linear Bathymetry z , 4.: Wave H and Velocities (uH, vH) for $t = 0.1$

Euler time-scheme and a DG-method of first order that was described before. For the spatial discretization, we have used $C_{IP} = 20$ in the SIPG method. Solving the state equations requires the definition of the time-horizon $T = 2.5$, which is chosen to include one full wave period, i.e. the travel of a wave to and from the shore. We have used a time-stepping size of $dt = 5e - 3$, which was calibrated in before each step such that we ensure not to violate the CFL-

condition, which is necessary for unconditionally stable marching procedures. Our calculations were performed for the test case of a linear decreasing bottom $z = 0.5 - 0.25y$. Having solved state and adjoint equations the mesh deformation is performed as described, where we specify $\mu_{min} = 10$ and $\mu_{max} = 100$ in (85) after projecting the solution from forward and backward problem to CG-elements. The step size is at $\rho = 1$ and shrinks whenever criteria for line searches are not met. In Figure 5 the result of optimizing the shape is displayed after 215 steps of optimization. The deformations appear to be symmetric. As we observe in Figure 6, we have achieved a notable

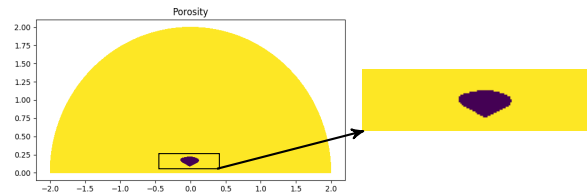


Figure 5: 1.: Optimized Shape of Porosity Region; 2.: Close up of Optimized Shape
decrease in the target functional.

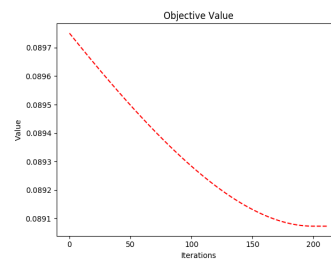


Figure 6: Target Function for Linear Seabed

5 CONCLUSION

We have investigated porous, viscous SWE, where the difference in the material coefficient can be interpreted as a permeable obstacle, that is placed in before shores. We have derived a well-balanced SIPG-DG scheme to solve for the evolution of the waves. Based on this solution we have derived the time-dependent continuous adjoint and shape derivative in volume form. Results were tested successfully on a simplistic sample mesh, where the obstacle's shape has been optimized to target a rest height at the shore. Results can be easily adjusted for arbitrary meshes, objective functions and different wave properties driven by initial and boundary conditions as partially shown in [27].

ACKNOWLEDGEMENT

This work has been supported by the Deutsche Forschungsgemeinschaft within the Priority program SPP 1962 "Non-smooth and Complementarity-based Distributed Parameter Systems: Simulation and Hierarchical Optimization". The authors would like to thank Diaraf Seck (Université Cheikh Anta

Diop, Dakar, Senegal) and Mame Gor Ngom (Université Cheikh Anta Diop, Dakar, Senegal) for helpful and interesting discussions within the project Shape Optimization Mitigating Coastal Erosion (SOMICE).

A APPENDIX

A.1 Derivation of Viscous Porous Momentum

We hereby follow [17] and extend for diffusive terms. In addition, we assume a water density $\rho = 1$ and remark that the volume V of water in a control volume is given by

$$V = \int_{y_0}^{y_0+\delta y} \int_{x_0}^{x_0+\delta x} \phi(x, y) H \, dx \, dy \quad (86)$$

with x_0, y_0 being the coordinates of the lower left corner of the control volume. Following [17] the momentum balance in x -direction can be written as

$$M = \frac{\partial M_x}{\partial t} - F_{M,W} + F_{M,E} - F_{M,S} + F_{M,N} - P_W + P_E - W_x - B_x - R_x = 0 \quad (87)$$

where F -terms account for x -Momentum fluxes, P -terms for pressure forces, such as W, B and R -terms for porosity influence such as bottom pressure and friction terms with indices representing the western W , eastern E northern N and southern S sides of the control volume. For viscous SWE as in [1] this momentum balance is extended by the volume diffusion through the western and eastern side as

$$D_W = - \int_{y_0}^{y_0+\delta y} \mu \phi H u_x(x_0, y) \, dy \quad (88)$$

$$D_E = - \int_{y_0}^{y_0+\delta y} \mu \phi H u_x(x_0 + \delta x, y) \, dy \quad (89)$$

such as southern and northern sides

$$D_S = - \int_{x_0}^{x_0+\delta x} \mu \phi H u_y(x, y_0) \, dx \quad (90)$$

$$D_N = - \int_{x_0}^{x_0+\delta x} \mu \phi H u_y(x, y_0 + \delta y) \, dx \quad (91)$$

where u_x and u_y denotes the first spatial derivatives with respect to x and y and diffusion coefficient μ . Momentum balancing these terms then leads to

$$M - D_W + D_E - D_S + D_N = 0 \quad (92)$$

Substituting terms in (92) gives

$$M + \int_{y_0}^{y_0+\delta y} \mu \phi H u_x(x_0, y) \, dy - \int_{y_0}^{y_0+\delta y} \mu \phi H u_x(x_0 + \delta x, y) \, dy + \quad (93)$$

$$\int_{x_0}^{x_0+\delta x} \mu \phi H u_y(x, y_0) \, dx - \int_{x_0}^{x_0+\delta x} \mu \phi H u_y(x, y_0 + \delta y) \, dx = 0 \quad (94)$$

when δx and δy tend to 0 it holds

$$\lim_{\delta x \rightarrow 0} (\mu \phi H u_x)(x_0 + \delta x, y) - (\mu \phi H u_x)(x_0, y) = \delta x \frac{\partial}{\partial x} (\mu \phi H u_x) \quad (95)$$

$$\lim_{\delta y \rightarrow 0} (\mu \phi H u_y)(x, y_0 + \delta y) - (\mu \phi H u_y)(x, y_0) = \delta y \frac{\partial}{\partial y} (\mu \phi H u_y) \quad (96)$$

Evaluating integrals leads to

$$\delta x \delta y M - \delta x \delta y \frac{\partial}{\partial x} (\mu \phi H u_x) - \delta x \delta y \frac{\partial}{\partial y} (\mu \phi H u_y) = 0 \quad (97)$$

which leads to the momentum balance as

$$M - \frac{\partial}{\partial x} (\mu \phi H u_x) - \frac{\partial}{\partial y} (\mu \phi H u_y) = 0 \quad (98)$$

The y-momentum is derived in accordance.

A.2 Derivation of Adjoint Equations

Proof. We need to perform integration by parts once more on (36) to obtain

$$\begin{aligned} a(H, \vec{Q}, p, \vec{r}) = & \int_0^T \int_{\Omega} -\frac{\partial p}{\partial t} \phi H \, dx \, dt + \int_{\Omega} \phi [H(T, x) p(T, x) - H_0 p(0, x)] \, dx + \\ & \int_0^T \int_{\Omega} -\phi \vec{Q} \cdot \nabla p \, dx \, dt + \int_0^T \int_{\Gamma_{out}} p \phi \vec{Q} \cdot \vec{n} \, ds \, dt + \\ & \int_0^T \int_{\Gamma_3} \llbracket p \phi \vec{Q} \cdot \vec{n} \rrbracket \, ds \, dt + \\ & \int_0^T \int_{\Omega} -(H+z) \nabla \cdot (\epsilon_v \nabla p) \, dx \, dt + \\ & \int_0^T \int_{\Gamma_{out}} [\epsilon_v (H+z) \nabla p \cdot \vec{n} - p \epsilon_v \nabla (H+z) \cdot \vec{n}] \, ds \, dt + \\ & \int_0^T \int_{\Gamma_3} \llbracket [\epsilon_v \nabla (H+z) \cdot \vec{n} p] - [\epsilon_v (H+z) \nabla p \cdot \vec{n}] \rrbracket \, ds \, dt + \\ & \int_0^T \int_{\Omega} -\frac{\partial \vec{r}}{\partial t} \cdot (\phi \vec{Q}) \, dx \, dt + \int_{\Omega} \phi [\vec{Q}(T, x) \cdot \vec{r}(T, x) - \vec{Q}_0 \cdot \vec{r}(0, x)] \, dx + \\ & \int_0^T \int_{\Omega} -\phi \frac{\vec{Q}}{H} \cdot \nabla \vec{r} \cdot \vec{Q} \, dx \, dt + \int_0^T \int_{\Gamma_{out}} \phi \frac{\vec{Q}}{H} \cdot \vec{r} \vec{Q} \cdot \vec{n} \, ds \, dt + \\ & \int_0^T \int_{\Omega} -\frac{1}{2} g \phi H^2 \nabla \cdot \vec{r} \, dx \, dt + \int_0^T \int_{\Gamma_{out}} \frac{1}{2} g \phi H^2 \vec{r} \cdot \vec{n} \, ds \, dt + \\ & \int_0^T \int_{\Gamma_3} \llbracket \phi \frac{\vec{Q}}{H} \cdot \vec{r} \vec{Q} \cdot \vec{n} \rrbracket \, ds \, dt + \int_0^T \int_{\Gamma_3} \llbracket \frac{1}{2} g \phi H^2 \vec{r} \cdot \vec{n} \rrbracket \, ds \, dt + \\ & \int_0^T \int_{\Omega} -\vec{Q} \cdot \nabla \cdot (\epsilon_f \phi \nabla \vec{r}) \, dx \, dt + \int_0^T \int_{\Omega} g \phi H \nabla z \cdot \vec{r} \, dx \, dt + \\ & \int_0^T \int_{\Gamma} [\epsilon_f \phi \vec{Q} \cdot \nabla \vec{r} \cdot \vec{n} - \vec{r} \cdot (\epsilon_f \phi \nabla \vec{Q}) \cdot \vec{n}] \, ds \, dt + \\ & \int_0^T \int_{\Gamma_3} \llbracket [\epsilon_f \phi \nabla (\vec{Q}) \cdot \vec{n} \cdot \vec{r}] - [\epsilon_f \phi \nabla \vec{r} \cdot \vec{Q} \cdot \vec{n}] \rrbracket \, ds \, dt - \\ & \int_0^T \int_{\Omega} g \frac{1}{2} H^2 \nabla \phi \cdot \vec{r} \, ds \, dt \end{aligned} \quad (99)$$

Using the jump identity $\llbracket ab \rrbracket = \{\{a\}\}\llbracket b \rrbracket + \{\{b\}\}\llbracket a \rrbracket$ and inserting Boundary Conditions on Γ_1 and Γ_2 such as on Γ_3 for the diffusive fluxes leads to

$$\begin{aligned}
a(H, \vec{Q}, p, \vec{r}) = & \int_0^T \int_{\Omega} -\frac{\partial p}{\partial t} \phi H \, dx \, dt + \int_{\Omega} \phi [H(T, x)p(T, x) - H_0 p(0, x)] \, dx - \\
& \int_0^T \int_{\Omega} \phi \vec{Q} \cdot \nabla p \, dx \, dt + \int_0^T \int_{\Gamma_2} \phi p \vec{Q} \cdot \vec{n} \, ds \, dt + \int_0^T \int_{\Gamma_3} \llbracket p \phi \vec{Q} \cdot \vec{n} \rrbracket \, ds \, dt - \\
& \int_0^T \int_{\Omega} \frac{1}{2} g \phi H^2 \nabla \cdot \vec{r} \, dx \, dt - \int_0^T \int_{\Omega} (H+z) \nabla \cdot (\epsilon_v \nabla p) \, dx \, dt + \\
& \int_0^T \int_{\Gamma_1} \epsilon_v (H+z) \nabla p \cdot \vec{n} \, ds \, dt + \int_0^T \int_{\Gamma_2} \epsilon_v H_1 \nabla p \cdot \vec{n} \, ds \, dt + \\
& \int_0^T \int_{\Gamma_2} -p \epsilon_v \nabla (H_1 + z) \cdot \vec{n} \, ds \, dt + \\
& \int_0^T \int_{\Gamma_3} [\{\{\epsilon_v \nabla (H+z) \cdot \vec{n}\}\} \llbracket p \rrbracket - \{\{H+z\}\} \llbracket \epsilon_v \nabla p \cdot \vec{n} \rrbracket] \, ds \, dt - \\
& \int_0^T \int_{\Omega} \frac{\partial \vec{r}}{\partial t} \cdot (\phi \vec{Q}) \, dx \, dt + \int_{\Omega} \phi [\vec{Q}(T, x) \cdot \vec{r}(T, x) - \vec{Q}_0 \cdot \vec{r}(0, x)] \, dx - \\
& \int_0^T \int_{\Omega} \phi \frac{\vec{Q}}{H} \cdot \nabla \vec{r} \cdot \vec{Q} \, dx \, dt + \int_0^T \int_{\Gamma_2} \phi \frac{\vec{Q}}{H_1} \cdot \vec{r} \vec{Q} \cdot \vec{n} \, ds \, dt + \\
& \int_0^T \int_{\Gamma_1} \frac{1}{2} g \phi H^2 \vec{r} \cdot \vec{n} \, ds \, dt + \int_0^T \int_{\Gamma_2} \frac{1}{2} g \phi H_1^2 \vec{r} \cdot \vec{n} \, ds \, dt + \\
& \int_0^T \int_{\Gamma_3} \llbracket \phi \frac{\vec{Q}}{H} \cdot \vec{r} \vec{Q} \cdot \vec{n} \rrbracket \, ds \, dt + \int_0^T \int_{\Gamma_3} \llbracket \frac{1}{2} g \phi H^2 \vec{r} \cdot \vec{n} \rrbracket \, ds \, dt - \\
& \int_0^T \int_{\Omega} (\vec{Q}) \cdot \nabla \cdot (\epsilon_f \phi \nabla \vec{r}) \, dx \, dt + \int_0^T \int_{\Gamma_1, \Gamma_2} \epsilon_f \phi \vec{Q} \nabla \vec{r} \cdot \vec{n} \, ds \, dt + \\
& \int_0^T \int_{\Gamma_3} [\{\{\epsilon_f \phi \nabla (\vec{Q}) \cdot \vec{n}\}\} \cdot \llbracket \vec{r} \rrbracket - \{\{\vec{Q}\}\} \cdot \llbracket \epsilon_f \phi \nabla \vec{r} \cdot \vec{n} \rrbracket] \, ds \, dt + \\
& \int_0^T \int_{\Omega} g \phi H \nabla z \cdot \vec{r} \, dx \, dt - \int_0^T \int_{\Omega} g \frac{1}{2} H^2 \nabla \phi \cdot \vec{r} \, dx \, dt
\end{aligned} \tag{100}$$

Differentiating for the state variables leads to

$$\begin{aligned}
\frac{\partial a(H, \vec{Q}, p, \vec{r})}{\partial H} = & \int_0^T \int_{\Omega} -\frac{\partial \phi p}{\partial t} \, dx \, dt + \int_{\Omega} \phi p(T, x) \, dx + \\
& \int_0^T \int_{\Omega} -\nabla \cdot (\epsilon_v \nabla p) \, dx \, dt + \int_0^T \int_{\Gamma_1} [\epsilon_v \nabla p \cdot \vec{n}] \, ds \, dt + \\
& \int_0^T \int_{\Gamma_3} [\{\{\epsilon_v \nabla (H+z) \cdot \vec{n}\}\}_H \llbracket p \rrbracket - \{\{H+z\}\}_H \llbracket \epsilon_v \nabla p \cdot \vec{n} \rrbracket] \, ds \, dt - \\
& \int_0^T \int_{\Omega} \phi \frac{\vec{Q}}{H^2} \cdot \nabla \vec{r} \cdot \vec{Q} \, dx \, dt - \\
& \int_0^T \int_{\Gamma_3} \llbracket \phi \frac{\vec{Q}}{H^2} \cdot \vec{r} \vec{Q} \cdot \vec{n} \rrbracket \, ds \, dt + \int_0^T \int_{\Gamma_3} \llbracket g \phi H \vec{r} \cdot \vec{n} \rrbracket \, ds \, dt - \\
& \int_0^T \int_{\Omega} -g \phi H \nabla \cdot \vec{r} \, dx \, dt + \int_0^T \int_{\Gamma_1} g \phi H \vec{r} \cdot \vec{n} \, ds \, dt + \\
& \int_0^T \int_{\Omega} g \phi \nabla z \cdot \vec{r} \, dx \, dt - \int_0^T \int_{\Omega} g H \nabla \phi \cdot \vec{r} \, dx \, dt
\end{aligned} \tag{101}$$

$$\begin{aligned}
\frac{\partial a(H, \vec{Q}, p, \vec{r})}{\partial \vec{Q}} &= \int_0^T \int_{\Omega} -\frac{\partial \phi \vec{r}}{\partial t} dx dt + \int_{\Omega} \phi \vec{r}(T, x) dx - \\
&\int_0^T \int_{\Omega} \phi \nabla p dx dt + \int_0^T \int_{\Gamma_2} \phi p \vec{n} ds dt + \int_0^T \int_{\Gamma_3} \llbracket p \phi \vec{n} \rrbracket \\
&\int_0^T \int_{\Omega} -\phi \frac{1}{H} (\nabla \vec{r})^T \vec{Q} - \frac{1}{H} (\vec{Q} \cdot \nabla) \vec{r} \vec{Q} dx dt + \\
&\int_0^T \int_{\Gamma_2} \frac{\phi}{H_1} (\vec{Q} \cdot \vec{n}) \vec{r} ds dt + \int_0^T \int_{\Gamma_2} \frac{\phi}{H_1} (\vec{Q} \vec{r}) \cdot \vec{n} ds dt + \\
&\int_0^T \int_{\Gamma_3} \llbracket \frac{\phi}{H} (\vec{Q} \cdot \vec{n}) \vec{r} \rrbracket ds dt + \int_0^T \int_{\Gamma_3} \llbracket \frac{\phi}{H} (\vec{Q} \vec{r}) \cdot \vec{n} \rrbracket ds dt - \\
&\int_0^T \int_{\Omega} \nabla \cdot (\epsilon_f \phi \nabla \vec{r}) dx dt + \int_0^T \int_{\Gamma_1, \Gamma_2} \epsilon_f \phi \nabla \vec{r} \vec{n} ds dt + \\
&\int_0^T \int_{\Gamma_3} \left[\{ \{ \epsilon_f \phi \nabla (\vec{Q}) \vec{n} \} \}_{\vec{Q}} \llbracket \vec{r} \rrbracket - \{ \{ \vec{Q} \} \}_{\vec{Q}} \llbracket \epsilon_f \phi \nabla \vec{r} \vec{n} \rrbracket \right] ds dt
\end{aligned} \tag{102}$$

Now if $\frac{\partial a(H, \vec{Q}, p, \vec{r})}{\partial U} = -\frac{\partial J_1}{\partial U}$ then $\frac{\partial \mathcal{L}}{\partial U} = 0$ is fulfilled. From this we get the adjoint equations in strong form (37) and (38) with boundary conditions from equating boundary terms to zero in (101) and (102). \square

A.3 Derivation of Shape Derivative

Proof. We regard the Lagrangian (35). As in [29], the theorem of Correa and Seger [11] is applied on the right hand side of

$$J_1(\Omega) = \min_U \max_P \mathcal{L}(\Omega, U, P) \tag{103}$$

The assumptions of this theorem can be verified as in [12]. We now apply the rule (28) for differentiating domain integrals

$$\begin{aligned}
d\mathcal{L}(\Omega, U, P) &= \lim_{\epsilon \rightarrow 0^+} \frac{\mathcal{L}(\Omega_{\epsilon}; U, P) - \mathcal{L}(\Omega; U, P)}{\epsilon} \\
&= \frac{d^+}{d\epsilon} \mathcal{L}(\Omega_{\epsilon}, U, P) \Big|_{\epsilon=0} = \frac{d^+}{d\epsilon} \mathcal{L}(\Omega_{\epsilon}, H, \vec{Q}, p, \vec{r}) \Big|_{\epsilon=0} \\
&= \int_{\Omega} \left[\int_0^T -D_m \left(\frac{\partial p}{\partial t} \phi H \right) dt + D_m (\phi H(T, x) p(T, x) - \phi H_0 p(0, x)) + \right. \\
&\quad \int_0^T -D_m \left(\frac{\partial \vec{r}}{\partial t} \cdot \phi \vec{Q} \right) dt + D_m (\phi \vec{Q}(T, x) \cdot \vec{r}(T, x) - \phi \vec{Q}_0 \cdot \vec{r}(0, x)) + \\
&\quad \int_0^T D_m (\nabla \cdot (\phi \vec{Q}) p) dt + \int_0^T D_m (\epsilon_v \nabla (H + z) \cdot \nabla p) dt + \\
&\quad \int_0^T D_m \left(\nabla \cdot \left(\phi \frac{\vec{Q}}{H} \otimes \vec{Q} \right) \cdot \vec{r} \right) dt + \int_0^T D_m \left(\frac{1}{2} g \nabla (\phi H^2) \cdot \vec{r} \right) dt + \\
&\quad \int_0^T D_m (\phi \epsilon_f \nabla \vec{Q} : \nabla \vec{r}) dt + \int_0^T D_m (g H \nabla z \cdot \vec{r}) dt + \\
&\quad \left. \int_0^T -D_m \left(\frac{1}{2} g H^2 \nabla \phi \cdot \vec{r} \right) dt + \right.
\end{aligned}$$

$$\begin{aligned}
 & \operatorname{div}(\vec{V}) \left(\int_0^T -\frac{\partial p}{\partial t} \phi H \, dt + \phi H(T, x) p(T, x) - \phi H_0 p(0, x) + \right. \\
 & \int_0^T -\frac{\partial \vec{r}}{\partial t} \cdot (\phi \vec{Q}) \, dt + \phi \vec{Q}(T, x) \cdot \vec{r}(T, x) - \phi \vec{Q}_0 \cdot \vec{r}(0, x) + \int_0^T \nabla \vec{Q} \cdot p \, dt + \\
 & \int_0^T \epsilon_v \nabla(H+z) \cdot \nabla p \, dt + \int_0^T \nabla \cdot \left(\phi \frac{\vec{Q}}{H} \otimes \vec{Q} \right) \cdot \vec{r} \, dt + \\
 & \int_0^T +\frac{1}{2} g \nabla(\phi H^2) \cdot \vec{r} \, dt + \int_0^T \phi \epsilon_f \nabla \vec{Q} : \nabla \vec{r} + \int_0^T g \phi H \nabla z \cdot \vec{r} \, dt - \\
 & \left. \int_0^T g H^2 \nabla \phi \cdot \vec{r} \, dt \right) dx + \int_{\Gamma_1} \left[\frac{1}{2} \int_0^T D_m \left([C(\hat{U}(t, x) - \tilde{U}(t, x))]^2 \right) + \right. \\
 & \left. \operatorname{div}_{\Gamma_1}(\vec{V}) [C(\hat{U}(t, x) - \tilde{U}(t, x))]^2 \, dt \right] ds - \\
 & \int_{\Gamma_2} \left[\int_0^T D_m (\epsilon_v \nabla(H_1 + z) \cdot \vec{n} p) \, dt + \operatorname{div}_{\Gamma_2}(\vec{V}) \left(\int_0^T \epsilon_v \nabla(H_1 + z) \cdot \vec{n} p \, dt \right) \right] ds - \\
 & \int_{\Gamma_3} \left[\int_0^T D_m (\llbracket \epsilon_v \nabla(H+z) \cdot \vec{n} p \rrbracket) \, dt + \int_0^T D_m (\llbracket \phi \epsilon_f \nabla \vec{Q} \cdot \vec{n} \cdot \vec{r} \rrbracket) \, dt + \right. \\
 & \left. \operatorname{div}_{\Gamma_3}(\vec{V}) \left(\int_0^T \llbracket -\epsilon_v \nabla(H+z) \cdot \vec{n} p \rrbracket \, dt + \int_0^T \llbracket -\phi \epsilon_f \nabla \vec{Q} \cdot \vec{n} \cdot \vec{r} \rrbracket \, dt \right) \right] ds
 \end{aligned}$$

where $\operatorname{div}_{\Gamma} \vec{V} = \operatorname{div} \vec{V} - \vec{n} \cdot (\nabla \vec{V}) \vec{n}$ is the tangential divergence of the vector field \vec{V} . Now the product rule (30) yields

$$\begin{aligned}
 & = \int_{\Omega} \left[\int_0^T -D_m \left(\frac{\partial p}{\partial t} \right) \phi H - \frac{\partial p}{\partial t} D_m(\phi H) \, dt + \right. \\
 & D_m(\phi H(T, x)) p(T, x) + H(T, x) \dot{p}(T, x) - \phi H_0 \dot{p}(0, x) + \\
 & \int_0^T -D_m \left(\frac{\partial \vec{r}}{\partial t} \right) \cdot (\phi \vec{Q}) - \frac{\partial \vec{r}}{\partial t} \cdot D_m(\phi \vec{Q}) \, dt + D_m(\vec{Q}(T, x)) \cdot \vec{r}(T, x) + \\
 & \phi \vec{Q}(T, x) \cdot \dot{\vec{r}}(T, x) - \phi \vec{Q}_0 \cdot \dot{\vec{r}}(0, x) + \int_0^T \dot{p} \cdot \nabla(\phi \vec{Q}) + p \cdot D_m(\nabla(\phi \vec{Q})) \, dt + \\
 & \int_0^T (\epsilon_v D_m(\nabla(H+z)) \cdot \nabla p + \epsilon_v \nabla(H+z) \cdot D_m(\nabla p)) \, dt - \\
 & \int_0^T D_m \left(\nabla \cdot \left(\phi \frac{\vec{Q}}{H} \otimes \vec{Q} \right) \right) \cdot \vec{r} \, dt + \int_0^T \nabla \cdot \left(\phi \frac{\vec{Q}}{H} \otimes \vec{Q} \right) \cdot D_m(\vec{r}) \, dt + \\
 & \int_0^T \left(\frac{1}{2} g D_m(\nabla(\phi H^2)) \cdot \vec{r} + \frac{1}{2} g \nabla(\phi H^2) \cdot D_m(\vec{r}) \right) \, dt + \\
 & \int_0^T \left(D_m(\phi \epsilon_f \nabla \vec{Q}) : \nabla \vec{r} + \phi \epsilon_f \nabla \vec{Q} : D_m(\nabla \vec{r}) \right) \, dt + \\
 & \int_0^T g D_m(\phi H) \nabla z \cdot \vec{r} \, dt + \int_0^T g \phi H D_m(\nabla z) \cdot \vec{r} \, dt + \int_0^T g \phi H \nabla z \cdot \dot{\vec{r}} \, dt - \\
 & \int_0^T \frac{1}{2} g D_m(H^2) \nabla \phi \cdot \vec{r} \, dt - \int_0^T \frac{1}{2} g H^2 D_m(\nabla \phi) \cdot \vec{r} \, dt - \int_0^T \frac{1}{2} g H^2 \nabla \phi \cdot \dot{\vec{r}} \, dt + \\
 & \operatorname{div}(\vec{V}) \left(\int_0^T -\frac{\partial p}{\partial t} \phi H \, dt + \phi H(T, x) p(T, x) - \phi H_0 p(0, x) + \right. \\
 & \int_0^T -\frac{\partial \vec{r}}{\partial t} \cdot (\phi \vec{Q}) \, dt + \phi \vec{Q}(T, x) \cdot \vec{r}(T, x) - \phi \vec{Q}_0 \cdot \vec{r}(0, x) + \int_0^T \nabla \vec{Q} \cdot p \, dt + \\
 & \int_0^T \epsilon_v \nabla(H+z) \cdot \nabla p \, dt + \int_0^T \nabla \cdot \left(\phi \frac{\vec{Q}}{H} \otimes \vec{Q} \right) \cdot \vec{r} \, dt + \\
 & \left. \int_0^T \frac{1}{2} g \nabla(\phi H^2) \cdot \vec{r} \, dt + \int_0^T \phi \epsilon_f \nabla \vec{Q} : \nabla \vec{r} + \int_0^T g \phi H \nabla z \cdot \vec{r} \, dt - \right.
 \end{aligned}$$

$$\begin{aligned}
& \int_0^T gH^2 \nabla \phi \cdot \vec{r} \, dt \Big) dx + \int_{\Gamma_1} \int_0^T \left[\text{div}_{\Gamma_1}(\vec{V}) [C(\hat{U}(t, x) - \bar{U}(t, x))]^2 \right] dt \, ds + \\
& \int_{\Gamma_2} \left[\int_0^T -\epsilon_v \nabla(H_1 + z) \cdot \vec{n} \dot{p} \, dt + \text{div}_{\Gamma_2}(\vec{V}) \left(\int_0^T -\epsilon_v \nabla(H_1 + z) \cdot \vec{n} p \, dt \right) \right] ds + \\
& \int_{\Gamma_3} \left[\int_0^T \llbracket -\epsilon_v D_m(\nabla(H + z)) \cdot \vec{n} p - \epsilon_v \nabla(H + z) \cdot \vec{n} \dot{p} \rrbracket dt + \right. \\
& \left. \int_0^T \llbracket -\phi \epsilon_f D_m(\nabla \vec{Q} \cdot \vec{n}) \cdot \vec{r} - \phi \epsilon_f \nabla \vec{Q} \cdot \vec{n} \cdot \dot{\vec{r}} \rrbracket dt + \right. \\
& \left. \text{div}_{\Gamma_3}(\vec{V}) \left(\int_0^T \llbracket -\epsilon_v \nabla(H + z) \cdot \vec{n} p \rrbracket dt + \int_0^T \llbracket -\phi \epsilon_f \nabla \vec{Q} \cdot \vec{n} \cdot \vec{r} \rrbracket dt \right) \right] ds
\end{aligned}$$

the non-commuting of the material derivative (31), (32) and (33) such as integration by parts, regrouping and the fact that sediment and the porosity moves along with the deformation leads to

$$\begin{aligned}
& = \int_{\Gamma_1} \int_0^T [C(\hat{U}(t, x) - \bar{U}(t, x))] \cdot \dot{U} \, dt \, ds + \\
& \int_{\Omega} \int_0^T \left[\left(-\phi \frac{\partial p}{\partial t} + \frac{\phi}{H^2} (\vec{Q} \cdot \nabla) \vec{r} \cdot \vec{Q} - g\phi H (\nabla \cdot \vec{r}) - \nabla \cdot (\epsilon_v \nabla p) + g\phi \nabla z \cdot \vec{r} \right) \dot{H} + \right. \\
& \left(-\phi \frac{\partial \vec{r}}{\partial t} - \nabla p - \frac{\phi}{H} (\vec{Q} \cdot \nabla) \vec{r} - \frac{\phi}{H} (\nabla \vec{r})^T \vec{Q} - (\nabla \cdot (\phi \epsilon_f \nabla \vec{r})) \right) \cdot \dot{\vec{Q}} + \\
& \left(\phi \frac{\partial H}{\partial t} + \nabla \cdot (\phi \vec{Q} - \epsilon_v \nabla(H + z)) \right) \dot{p} + \\
& \left(\phi \frac{\partial \vec{Q}}{\partial t} + \nabla \cdot \left(\phi \frac{\vec{Q}}{H} \otimes \vec{Q} + \frac{1}{2} g\phi H^2 \mathbf{I} - \phi \epsilon_f \nabla \vec{Q} \right) + g\phi H \nabla z \right) \cdot \dot{\vec{r}} \Big] dx + \\
& \int_0^T \int_{\Omega} \left[-(\nabla \vec{V})^T : \nabla(\phi \vec{Q}) p - (\nabla \vec{V})^T : \nabla \vec{Q} \frac{\phi \vec{Q}}{H} \cdot \vec{r} - \right. \\
& (\nabla \vec{V} \vec{Q} \cdot \nabla) \frac{\phi \vec{Q}}{H} \cdot \vec{r} - gH (\nabla \vec{V})^T \nabla(\phi H) \cdot \vec{r} - \\
& \epsilon_v \nabla(H + z)^T (\nabla \vec{V} + \nabla \vec{V}^T) \nabla p - \\
& \phi \epsilon_f \nabla \vec{Q} \nabla \vec{V} : \nabla \vec{r} - \phi \epsilon_f \nabla \vec{Q} \nabla \vec{V}^T : \nabla \vec{r} - \\
& g\phi H \nabla \vec{V}^T \nabla z \cdot \vec{r} + \frac{1}{2} gH^2 \nabla \vec{V}^T \nabla \phi \cdot \vec{r} \\
& \left. \text{div}(\vec{V}) \left\{ \frac{\partial \phi H}{\partial t} p + \nabla \cdot (\phi \vec{Q}) p + \frac{\partial \phi \vec{Q}}{\partial t} \cdot \vec{r} + \right. \right. \\
& \left. \left. \phi (\vec{Q} \cdot \nabla) \frac{\vec{Q}}{H} \cdot \vec{r} + \nabla \cdot (\phi \vec{Q}) \frac{\vec{Q}}{H} \cdot \vec{r} + \frac{1}{2} g \nabla(\phi H^2) \cdot \vec{r} + \right. \right. \\
& \left. \left. g\phi H \nabla z \cdot \vec{r} + \epsilon_v \nabla(H + z) \cdot \nabla p + \right. \right. \\
& \left. \left. \phi \epsilon_f \nabla \vec{Q} : \nabla \vec{r} - g \frac{1}{2} H^2 \nabla \phi \cdot \vec{r} \right\} \right] dx \, dt \\
& \int_{\Gamma_1} \int_0^T \left[\text{div}_{\Gamma_1}(\vec{V}) [C(\hat{U}(t, x) - \bar{U}(t, x))]^2 \right] dt \, ds + \\
& \int_{\Gamma_3} \left[\int_0^T \left(\llbracket \frac{\phi \vec{Q}}{H} \cdot \vec{r} \vec{Q} \cdot \vec{n} + \frac{\phi \vec{Q}}{H} \cdot \vec{r} \dot{\vec{Q}} \cdot \vec{n} + p \phi \dot{\vec{Q}} \cdot \vec{n} + \right. \right. \\
& \left. \left. \int_0^T \frac{1}{2} g D_m(\phi H^2) \vec{r} \cdot \vec{n} \rrbracket dt \right) \right] ds + \\
& \text{div}_{\Gamma_3}(\vec{V}) \left(\int_0^T \llbracket -\epsilon_v \nabla(H + z) \cdot \vec{n} p \rrbracket dt + \int_0^T \llbracket -\phi \epsilon_f \nabla \vec{Q} \cdot \vec{n} \cdot \vec{r} \rrbracket dt \right) \Big] ds
\end{aligned}$$

Since outer boundaries are not variable, the deformation field \vec{V} vanishes in small neighbourhoods around Γ_1, Γ_2 and the material derivative is zero, hence the respective boundary integrals vanish. In addition, evaluating the Lagrangian in its saddle point, the first integral vanishes such that we obtain the shape derivative in its final form (52). Finally due to the continuity of the state and of the fluxes their material derivative is continuous and terms on Γ_3 vanish. \square

A.4 Derivation of DG Scheme for Interface Conditions

The porous SWE (1) together with interface conditions on Γ_3 lead to a DG-scheme. Starting from the weak form (36) and integrating by parts once more on the advective terms, in addition to once more using the jump identity $\llbracket ab \rrbracket = \{\{a\}\}\llbracket b \rrbracket + \{\{b\}\}\llbracket a \rrbracket$ together with flux continuity for the diffusive and advective flux we obtain

$$\begin{aligned}
a(H, \vec{Q}, p, \vec{r}) = & \int_0^T \int_{\Omega} -\frac{\partial p}{\partial t} \phi H \, dx \, dt + \int_{\Omega} \phi [H(T, x)p(T, x) - H_0 p(0, x)] \, dx + \\
& \int_0^T \int_{\Omega} -\phi \vec{Q} \cdot \nabla p \, dx \, dt + \int_0^T \int_{\Gamma_{out}} p \phi \vec{Q} \cdot \vec{n} \, ds \, dt + \\
& \int_0^T \int_{\Gamma_3} \{\{\phi \vec{Q} \cdot \vec{n}\}\} \llbracket p \rrbracket \, ds \, dt + \\
& \int_0^T \int_{\Omega} \epsilon_v \nabla(H+z) \cdot \nabla p \, dx \, dt - \\
& \int_0^T \int_{\Gamma_{out}} [p \epsilon_v \nabla(H+z) \cdot \vec{n}] \, ds \, dt - \\
& \int_0^T \int_{\Gamma_3} [\{\{\epsilon_v \nabla(H+z) \cdot \vec{n}\}\} \llbracket p \rrbracket] \, ds \, dt - \\
& \int_0^T \int_{\Omega} -\frac{\partial \vec{r}}{\partial t} \cdot (\phi \vec{Q}) \, dx \, dt + \int_{\Omega} \phi [\vec{Q}(T, x) \cdot \vec{r}(T, x) - \vec{Q}_0 \cdot \vec{r}(0, x)] \, dx + \\
& \int_0^T \int_{\Omega} -\phi \frac{\vec{Q}}{H} \cdot \nabla \vec{r} \cdot \vec{Q} \, dx \, dt + \int_0^T \int_{\Gamma_{out}} \phi \frac{\vec{Q}}{H} \cdot \vec{r} \vec{Q} \cdot \vec{n} \, ds \, dt + \\
& \int_0^T \int_{\Omega} -\frac{1}{2} g \phi H^2 \nabla \cdot \vec{r} \, dx \, dt + \int_0^T \int_{\Gamma_{out}} \frac{1}{2} g \phi H^2 \vec{r} \cdot \vec{n} \, ds \, dt + \\
& \int_0^T \int_{\Gamma_3} \{\{\phi (\frac{\vec{Q}}{H} \otimes \vec{Q}) \vec{n}\}\} \cdot \llbracket \vec{r} \rrbracket \, ds \, dt + \int_0^T \int_{\Gamma_3} \{\{\frac{1}{2} g \phi H^2 \vec{n}\}\} \cdot \llbracket \vec{r} \rrbracket \, ds \, dt + \\
& \int_0^T \int_{\Omega} \epsilon_f \phi \nabla \vec{Q} : \nabla \vec{r} \, dx \, dt + \int_0^T \int_{\Omega} g \phi H \nabla z \cdot \vec{r} \, dx \, dt - \\
& \int_0^T \int_{\Gamma} [\vec{r} \cdot \epsilon_f \phi \nabla \vec{Q} \cdot \vec{n}] \, ds \, dt - \\
& \int_0^T \int_{\Gamma_3} [\{\{\epsilon_f \phi \nabla \vec{Q} \cdot \vec{n}\}\} \cdot \llbracket \vec{r} \rrbracket] \, ds \, dt - \\
& \int_0^T \int_{\Omega} g \frac{1}{2} H^2 \nabla \phi \cdot \vec{r} \, ds \, dt
\end{aligned} \tag{104}$$

Since this derivation does not make use of the continuity of the solution, we weakly enforce it by adding

$$\int_0^T \int_{\Gamma_3} \underline{\delta}(\hat{U}) : \llbracket P \rrbracket \, ds \, dt \tag{105}$$

for

$$\delta_h(\hat{U}) = C_{IP} \frac{p^2}{h} \{ \{ G(f(\phi, \epsilon)) \} \} \llbracket \hat{U} \rrbracket \quad (106)$$

In addition, it appears natural to symmetrize the diffusive part by

$$- \int_0^T \int_{\Gamma_3} \{ \{ G(f(\phi, \epsilon)) \nabla(P) \} \} : \llbracket \hat{U} \rrbracket \quad (107)$$

For the advective-flux we can refer to upwinding as

$$\{ \{ \phi F(U) \cdot \vec{n} \} \}_{U_p} = \frac{1}{2} [\phi^+ F(U^+) \cdot \vec{n} + \phi^- F(U^-) \cdot \vec{n}] \quad (108)$$

Finally a complete DG-scheme over Ω_h is obtained by allowing discontinuous cell-transitions, performing integration and integration by parts on each cell. If we allow alternation in the usage of the numerical flux function \mathcal{H} we obtain the DG-scheme in known form (57)

A.5 Numerical Convergence of the Smoothed Approach

As mentioned in Section 4.2 the numerical scheme used to handle discontinuous sediment and porosity coefficients forms the limit of a smoothed scenario. We numerically justify this by relying the smoothed porosity on smoothed step functions in one dimension, i.e. for discontinuities located at $x_0 < x_1 \in \mathbb{R}$ the smoothed porosity is obtained from

$$\phi_\alpha(x) = [1 - d(x, \alpha)] \phi_2 + d(x, \alpha) \quad (109)$$

where

$$d(x, \alpha) = \begin{cases} 1 & \text{if } x \leq x_0 - \alpha \wedge x \geq x_1 + \alpha \\ -\frac{1}{4} \left(\frac{x_0 - x}{\alpha} \right)^3 + \frac{3}{4} \frac{x_0 - x}{\alpha} + \frac{1}{2} & \text{if } x > x_0 - \alpha \wedge x < x_0 + \alpha \\ 1 - \left(-\frac{1}{4} \left(\frac{x_1 - x}{\alpha} \right)^3 + \frac{3}{4} \frac{x_1 - x}{\alpha} + \frac{1}{2} \right) & \text{if } x > x_1 - \alpha \wedge x < x_1 + \alpha \\ 0 & \text{if } x \geq x_0 + \alpha \wedge x \leq x_1 - \alpha \end{cases} \quad (110)$$

We can observe exemplifications for varying α in Figure 7. Defining error

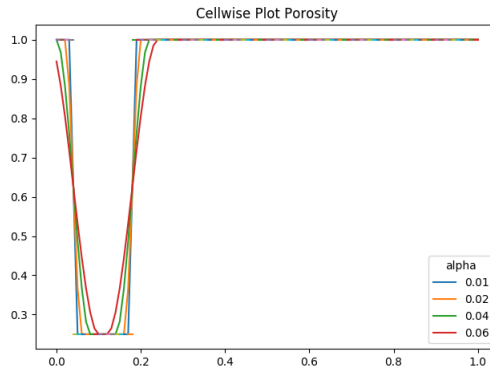


Figure 7: Examples of Smoothed Porosity

norms for water height H and weighted velocity uH as

$$E_H = \|H - H_\alpha\| = \left(\int_0^T \int_{\Omega} (H - H_\alpha)^2 dx dt \right)^{1/2} \quad (111)$$

$$E_{uH} = \|uH - uH_\alpha\| = \left(\int_0^T \int_\Omega (uH - uH_\alpha)^2 dx dt \right)^{1/2} \quad (112)$$

From construction of the well-balanced scheme it is obvious that steady state conditions $uH = 0$ for $H + z = C$ lead to zero error norms, since porosity smoothing leads to continuous cell-transitions, i.e. $\phi_h(x_{j+1/2}^-) = \phi_h(x_{j+1/2}^+)$. We hence exemplifying investigate Gaussian initial conditions for the surface height H , i.e. $(H_0, uH_0) = (1 + 0.3 \exp(-100(x - 1/2)^2), 0)$, over a time horizon of $T = 0.4$ and $dt = 0.001$. We can observe the convergence numerically $U = \lim_{\alpha \rightarrow 0} U_\alpha$ for $\phi = \lim_{\alpha \rightarrow 0} \phi_\alpha$ as shown in table 1. At this point, would like to emphasise that the convergence is limited by the grid size of the mesh, hence showing the limit decrease for $\alpha \rightarrow 0$ is only possible for $h \rightarrow 0$.

α	$\ H - H_\alpha\ $	$\ uH - uH_\alpha\ $
0.06	3.45587	8.41055
0.04	2.05134	4.69693
0.03	1.40056	3.08506
0.02	0.81980	1.69824
0.01	0.3443	0.601958
0.005	0.17583	0.23194
0.001	0.10549	0.11108

Table 1: Error Norms E_H and E_{uH} for decreasing α

REFERENCES

- [1] V.I. Agoshkov, A. Quarteroni, and F. Saleri. “Recent developments in the numerical simulation of shallow water equations I: boundary conditions”. In: *Applied Numerical Mathematics* 15.2 (1994), pp. 175–200. ISSN: 0168-9274. DOI: [https://doi.org/10.1016/0168-9274\(94\)00014-X](https://doi.org/10.1016/0168-9274(94)00014-X). URL: <http://www.sciencedirect.com/science/article/pii/016892749400014X>.
- [2] Vadym Aizinger and Clint Dawson. “A discontinuous Galerkin method for two-dimensional flow and transport in shallow water”. In: *Advances in Water Resources* 25.1 (2002), pp. 67–84. ISSN: 0309-1708. DOI: [https://doi.org/10.1016/S0309-1708\(01\)00019-7](https://doi.org/10.1016/S0309-1708(01)00019-7). URL: <http://www.sciencedirect.com/science/article/pii/S0309170801000197>.
- [3] Grégoire Allaire, François Jouve, and Georgios Michailidis. “Thickness control in structural optimization via a level set method”. In: *Structural and Multidisciplinary Optimization* 53 (June 2016). DOI: [10.1007/s00158-016-1453-y](https://doi.org/10.1007/s00158-016-1453-y).
- [4] Emmanuel Audusse, Christophe Chalons, and Philippe Ung. “A simple three-wave Approximate Riemann Solver for the Saint-Venant–Exner equations”. In: *International Journal for Numerical Methods in Fluids* (Sept. 2015). DOI: [10.1002/flid.4500](https://doi.org/10.1002/flid.4500).
- [5] Pascal Azerad et al. “Optimal Shape Design of Coastal Structures Minimizing Coastal Erosion”. In: *Extended Proceedings of Workshop on Inverse Problems*. Jan. 2005.
- [6] Adhémar-Jean-Claude Barré de Saint-Venant. “Théorie du mouvement non-permanent des eaux, avec application aux crues des rivières et à l’introduction des marées dans leur lit”. In: *C. R. Acad Sci Paris* (Aug. 1871).
- [7] Martin Berggren. “A Unified Discrete–Continuous Sensitivity Analysis Method for Shape Optimization”. In: vol. 15. Aug. 2010, pp. 25–39. DOI: [10.1007/978-90-481-3239-3_4](https://doi.org/10.1007/978-90-481-3239-3_4).
- [8] Alfredo Bermudez and Ma Elena Vazquez. “Upwind methods for hyperbolic conservation laws with source terms”. In: *Computers & Fluids* 23.8 (1994), pp. 1049–1071. ISSN: 0045-7930. DOI: [https://doi.org/10.1016/0045-7930\(94\)90004-3](https://doi.org/10.1016/0045-7930(94)90004-3). URL: <https://www.sciencedirect.com/science/article/pii/0045793094900043>.
- [9] Afaf Bouharguane and Bijan Mohammadi. “Minimization principles for the evolution of a soft sea bed interacting with a shallow”. In: *International Journal of Computational Fluid Dynamics* 26 (Mar. 2012), pp. 163–172. DOI: [10.1080/10618562.2012.669831](https://doi.org/10.1080/10618562.2012.669831).
- [10] Kyung K. Choi. “Shape Design Sensitivity Analysis and Optimal Design of Structural Systems”. In: *Computer Aided Optimal Design: Structural and Mechanical Systems*. Ed. by Carlos A. Mota Soares. Berlin, Heidelberg: Springer Berlin Heidelberg, 1987, pp. 439–492. ISBN: 978-3-642-83051-8.
- [11] Rafael Correa and Alberto Seeger. “Directional derivative of a minmax function”. In: *Nonlinear Analysis-theory Methods & Applications* 9 (Jan. 1985), pp. 13–22. DOI: [10.1016/0362-546X\(85\)90049-5](https://doi.org/10.1016/0362-546X(85)90049-5).

- [12] M. C. Delfour and J. -P. Zolésio. *Shapes and Geometries*. Second. Society for Industrial and Applied Mathematics, 2011. DOI: [10.1137/1.9780898719826](https://doi.org/10.1137/1.9780898719826). eprint: <https://epubs.siam.org/doi/pdf/10.1137/1.9780898719826>. URL: <https://epubs.siam.org/doi/abs/10.1137/1.9780898719826>.
- [13] Benjamin Dewals et al. “Porosity Models for Large-Scale Urban Flood Modelling: A Review”. In: *Water* 13.7 (2021). ISSN: 2073-4441. DOI: [10.3390/w13070960](https://doi.org/10.3390/w13070960). URL: <https://www.mdpi.com/2073-4441/13/7/960>.
- [14] Christophe Geuzaine and Jean-François Remacle. “Gmsh: A 3-D Finite Element Mesh Generator with Built-in Pre- and Post-Processing Facilities”. In: *International Journal for Numerical Methods in Engineering* 79 (Sept. 2009), pp. 1309–1331. DOI: [10.1002/nme.2579](https://doi.org/10.1002/nme.2579).
- [15] L. Gosse. “A well-balanced flux-vector splitting scheme designed for hyperbolic systems of conservation laws with source terms”. In: *Computers & Mathematics with Applications* 39.9 (2000), pp. 135–159. ISSN: 0898-1221. DOI: [https://doi.org/10.1016/S0898-1221\(00\)00093-6](https://doi.org/10.1016/S0898-1221(00)00093-6). URL: <https://www.sciencedirect.com/science/article/pii/S0898122100000936>.
- [16] Oksana Guba et al. “The spectral element method (SEM) on variable-resolution grids: Evaluating grid sensitivity and resolution-aware numerical viscosity”. In: *Geoscientific Model Development Discussions* 7 (June 2014). DOI: [10.5194/gmdd-7-4081-2014](https://doi.org/10.5194/gmdd-7-4081-2014).
- [17] Vincent Guinot and Sandra Soares-Frazão. “Flux and source term calculation in two-dimensional shallow water models with porosity on unstructured grids”. In: *International Journal for Numerical Methods in Fluids* 50 (Jan. 2006), pp. 309–345. DOI: [10.1002/flid.1059](https://doi.org/10.1002/flid.1059).
- [18] Ralf Hartmann. “Numerical Analysis of Higher Order Discontinuous Galerkin Finite Element Methods”. In: (Oct. 2008).
- [19] Paul Houston and Nathan Sime. *Automatic symbolic computation for discontinuous Galerkin finite element methods*. 2018. arXiv: [1804.02338](https://arxiv.org/abs/1804.02338) [cs.NA].
- [20] Damien Isebe et al. “Shape optimization of geotextile tubes for sandy beach protection”. In: *International Journal for Numerical Methods in Engineering* 74 (May 2008), pp. 1262–1277. DOI: [10.1002/nme.2209](https://doi.org/10.1002/nme.2209).
- [21] Tuomas Kärnä et al. “A fully implicit wetting–drying method for DG-FEM shallow water models, with an application to the Scheldt Estuary”. In: *Computer Methods in Applied Mechanics and Engineering* 200.5 (2011), pp. 509–524. ISSN: 0045-7825. DOI: <https://doi.org/10.1016/j.cma.2010.07.001>. URL: <http://www.sciencedirect.com/science/article/pii/S0045782510002136>.
- [22] Moritz Keuthen and D. Kraft. “Shape Optimization of a Breakwater”. In: *Inverse Problems in Science and Engineering* 24 (Sept. 2015). DOI: [10.1080/17415977.2015.1077522](https://doi.org/10.1080/17415977.2015.1077522).
- [23] Abdul Khan and Wencong Lai. *Modeling Shallow Water Flows Using the Discontinuous Galerkin Method*. Mar. 2014. ISBN: 9780429157936. DOI: [10.1201/b16579](https://doi.org/10.1201/b16579).
- [24] Bijan Mohammadi and Afaf Bouharguane. “Optimal dynamics of soft shapes in shallow waters”. In: *Computers & Fluids* 40 (Jan. 2011), pp. 291–298. DOI: [10.1016/j.compfluid.2010.09.031](https://doi.org/10.1016/j.compfluid.2010.09.031).

- [25] Joseph Oliger and Arne Sundström. “Theoretical and Practical Aspects of Some Initial Boundary Value Problems in Fluid Dynamics”. In: *SIAM Journal on Applied Mathematics* 35:3 (1978), pp. 419–446. DOI: [10.1137/0135035](https://doi.org/10.1137/0135035). eprint: <https://doi.org/10.1137/0135035>. URL: <https://doi.org/10.1137/0135035>.
- [26] Per-Olof Persson and J. Peraire. “Sub-Cell Shock Capturing for Discontinuous Galerkin Methods”. In: *AIAA paper* 2 (Jan. 2006). DOI: [10.2514/6.2006-112](https://doi.org/10.2514/6.2006-112).
- [27] Luka Schlegel and Volker Schulz. *Shape Optimization for the Mitigation of Coastal Erosion via Shallow Water Equations*. 2021. arXiv: [2107.09464](https://arxiv.org/abs/2107.09464) [math.OC].
- [28] Volker Schulz and Martin Siebenborn. *Computational comparison of surface metrics for PDE constrained shape optimization*. 2016. arXiv: [1509.08601](https://arxiv.org/abs/1509.08601) [math.OC].
- [29] Volker Schulz, Martin Siebenborn, and Kathrin Welker. “Structured inverse modeling in parabolic diffusion processes”. In: *SIAM Journal on Control and Optimization* 53 (Sept. 2014). DOI: [10.1137/140985883](https://doi.org/10.1137/140985883).
- [30] Volker H. Schulz, Martin Siebenborn, and Kathrin Welker. “Efficient PDE Constrained Shape Optimization Based on Steklov–Poincaré-Type Metrics”. In: *SIAM Journal on Optimization* 26.4 (2016), pp. 2800–2819. DOI: [10.1137/15M1029369](https://doi.org/10.1137/15M1029369). eprint: <https://doi.org/10.1137/15M1029369>. URL: <https://doi.org/10.1137/15M1029369>.
- [31] J. Sokołowski and J.P. Zolésio. *Introduction to shape optimization: shape sensitivity analysis*. Springer series in computational mathematics. Springer-Verlag, 1992. ISBN: 9783540541776. URL: <https://books.google.de/books?id=hg-oAAAAIAAJ>.
- [32] Kathrin Welker. “Efficient PDE Constrained Shape Optimization in Shape Spaces”. doctoralthesis. Universität Trier, 2017. DOI: [10.25353/ubtr-xxxx-6575-788c/](https://doi.org/10.25353/ubtr-xxxx-6575-788c/).
- [33] Yulong Xing and Chi-Wang Shu. “A New Approach of High Order Well-Balanced Finite Volume WENO Schemes and Discontinuous Galerkin Methods for a Class of Hyperbolic Systems with Source”. In: *Communications in Computational Physics* 1 (Feb. 2006).